Marine Structures 40 (2015) 1–37

Contents lists available at ScienceDirect

Marine Structures

journal homepage: www.elsevier.com/locate/marstruc

Energy dissipation in high-energy ship-offshore jacket platform collisions

Joao Travanca [a, *], Hong Hao [b]

[a] School of Civil and Resource Engineering, The University of Western Australia, 35 Stirling Highway, Crawley WA 6009, Australia
[b] Department of Civil Engineering, Curtin University, Kent St., Bentley WA 6102, Australia

ARTICLE INFO

Article history:
Received 20 May 2014
Received in revised form 28 August 2014
Accepted 3 October 2014
Available online

Keywords:
Ship impact
Ship-platform interaction
Strain energy dissipation
Relative strength
Finite element analysis

ABSTRACT

Ship collisions with offshore structures may be characterized by large amounts of kinetic energy that can be dissipated as strain energy in either the ship, or the installation, or shared by both. In this paper a series of FE numerical simulations are performed with the aim of providing a clearer understanding on the strain energy dissipation phenomenon, particularly upon the ship-structure interaction. Ships of different dimensions and layouts are modelled for impact simulations. Likewise, three platform jacket models of different sizes and configurations are considered. The collision cases involve joints, legs, and braces and are simulated for several kinetic energy amounts of the vessels and different impact orientations. An overview of the plastic deformation mechanisms that can occur in both ship and jacket structure is also given. The results from the various models with different collision scenarios are compared in terms of the strain energy dissipation with respect to the different ship/installation strength ratios. From the FEA simplified approaches are also derived in terms of the relative stiffness of the two structures for assessing the responses and energy absorptions of the two structures. The conclusions drawn from this study can be applied to a broader range of collision assessment of offshore steel jacket platforms subjected to high-energy ship impacts.

© 2014 Elsevier Ltd. All rights reserved.

* Corresponding author. Tel.: +61 8 6488 3974; fax: +61 8 6488 1044.
E-mail address: joao@civil.uwa.edu.au (J. Travanca).

http://dx.doi.org/10.1016/j.marstruc.2014.10.008
0951-8339/© 2014 Elsevier Ltd. All rights reserved.

1. Introduction

The ship collision evaluation often includes impact events between the offshore installation and nearby vessels subject of off-loading strike. A risk assessment usually needs to be carried out for potential collision events that are screened according to their risk for the structure and also to their likelihood. For the assessment process, the failure shall be considered for members individually or by means of the overall performance of the facility, i.e. keeping the structure functional after, for instance, rupturing of a brace or denting of a leg. During the impact, the kinetic energy of the striking ship is converted into strain energy of the vessel and the facility (that can be either fixed or floating). Some of the energy might also remain associated with the motion of the structures after the impact (rebound). It is therefore important to account for the plastic deformation and failure of structural members that are affected by the collision since they will generally be associated with the primary structural effects. Fixed platforms are typically lower in redundancy than the floating ones and also constitute the most representative offshore structures [1,2]. Likewise, the acceptance criteria defined for each type is also different. As for the energy amounts specified for the collision assessment, these are derived from both vessel size and impact speed. Collision events involving supply vessels are currently predicted for ship sizes up to 5000 ton [3], although these have significant variations in size according to the region they operate [4,5], while for the impact velocity these might range from 0.5 m/s for low-energy collision to 2 m/s for drifting supply vessels [4]. The combination between these two factors can actually result in large amounts of energy especially if the incidents involving passing vessels (reported in Ref. [6]) are considered, as well as a plausible increase in the number and average size of the world's fleet in the coming years.

For the evaluation of the structural damage via energy balance, the internal energy consists of contributions from both the vessel and installation strain energy. Such contributions might vary upon the relative strength between the two structures. The methods used to estimate the strain energy in the current design practice can be very conservative because of neglecting the ship-platform interaction through the assumption of the ship to be rigid and the entire strain energy from the installation deformation, or less conservative, by analysing ship and platform being collided by a rigid body separately. For the latter case, the strain energy from the vessel, as well as the associated damage to it is usually underestimated same is the correspondent applied load. To improve the prediction accuracy, the high fidelity FEA provides a mean to perform the coupled analyses by simultaneously considering deformations of both the facility and ship, and including their interaction. This approach gains significance, in particular for cases where greater energy amounts than those currently predicted by the design practice, since a better accuracy could allow for a less conservative solution.

2. Energy absorption

Even though the elastic stiffness of the structures involved in the collision can affect the energy dissipation process, for high energy collisions the plastic deformations will absorb most of the initial kinetic energy, considering that the ship rebound will not be significant. Besides the global elastic vibrations of the installation, different plastic mechanisms can be formed locally on both ship and offshore facility depending on the collision scenario. The contribution of each of such modes is normally determined upon simplified hand calculation methods that can be found throughout the literature.

2.1. Local denting and beam bending

For beams subjected to transverse loads, there are two mechanisms, i.e., beam bending and tube wall denting, which can interact with each other (Fig. 1). While global bending might govern the deformation of braces, legs are usually designed against local denting. Extensive literature can be found with respect to the beam flexural behaviour under transverse loading and in particular for steel tubular members.

The plastic force-deformation relationships for local denting of tubes are normally modelled by an equivalent spring determined according to the mechanical and geometrical properties of the tube. The

Fig. 1. Tube deformation under lateral transverse loading.

energy absorbed due to local denting is then evaluated through integration of the force-deformation curve of the spring. Commonly referred relationships for the prediction of the tube lateral response are those formulated by Furnes and Amdahl [7] and Ellinas and Walker [8]. The two equations however may yield significantly different energy and impact force values depending on the different D/t ratios used. Additional studies considered the variations on the striker shape [9] or the influence of dynamic effects [10]. Some experimental tests can also be found in the literature [11,12]. The extension of the dent is another important parameter in the assessment of the plastic strain energy and it becomes more relevant for the ship impact case due to the large contact areas involved. The influences of these parameters are included in the integrated expression of the denting deformation and energy absorption described in the DNV code [3], given as:

$$\frac{E_d}{R_c} = c_1 \cdot \left(\frac{x^{c_2+1}}{c_2+1}\right) \cdot \left(\frac{1}{D}\right)^{c_2} \tag{1}$$

$$c_1 = \left(22 + 1.2 \cdot \frac{b}{D}\right) \cdot c_3 \tag{2}$$

$$c_2 = \frac{1.925}{3.5 + \frac{b}{D}} \tag{3}$$

$$c_3 = 1.0, \quad \frac{N_{Sd}}{N_{Rd}} \leq 0.2 \tag{4}$$

$$R_c = \sigma_y \frac{t^2}{4} \sqrt{\frac{D}{t}} \tag{5}$$

where b is the dent length along the tube longitudinal direction, D the tube diameter, t the tube thickness, σ_y the yield stress, E_d the amount of absorbed strain energy from the dent, and N_{Sd} and N_{Rd} the design axial compressive force and capacity, respectively. It should be noted that Equation (1) may yield inaccurate predictions of strain energy absorptions in evaluating ship bow impacts on leg platforms because it was derived based on a flat impact area while the ship bow impact indentation is characterized with irregular shapes, especially if both bulb and forecastle deck hit the tube.

For tubular beams undergoing large deformations the global bending response is estimated using the three-hinge mechanism [13] based on the principle of virtual works. The load is modelled as a concentrated load. The effects of axial flexibility of the supports and the strength of the connections can be also included by introducing additional elements with the equivalent axial strength of the adjacent structural members. The interaction of global bending with local denting can also be taken into consideration based on the assumption that the indented area is flat and the remaining part of the cross section has a constant radius of curvature. The reduced plastic section modulus can then be derived from integration of the deformed cross section.

Despite the combined occurrence of local denting and beam bending, the contribution of the two different modes in terms of energy absorption is not of easy estimation. Procedures based on idealized cross-section deformation upon penetration of regular shape indenters [12] have been proved to be inaccurate for denting values lower than 30% of the diameter of the intact cross section [14], especially when the contact areas with the striker are irregular. However, in Ref. [14] it is shown that the amount of strain energy dissipated by the tubes can be predicted based on the total displacement of the membrane in contact with the striker, regardless of whether bending or denting govern the tube deformation. However, the accuracy of this observation depends on the extent of the contact area. It can equally be assumed that if the energy of the collision is written in its non-dimensional form considering only the strain energy of the tube, the same predictions can be performed regardless of the striker deformation. The dimensionless energy is then defined with respect to the static collapse load of a circular tube in pure bending P_u (valid as long as no buckling of the tube wall and the full plastic capacity of the cross section is achieved during the deformation), as:

$$\lambda = \frac{E}{P_u t} = \frac{LE}{8\sigma_y D^2 t^2} \tag{6}$$

where $P_u t$ represents the external work of the concentrated collapse load P_u that produces a transverse displacement equal to t right underneath the load application point. Similarly to [14], the dimensionless energies here are evaluated from the strain energy of the platform rather than the initial kinetic energy of the striker.

2.2. Axial crushing and buckling

The study of crushing mechanics of thin-walled structures has had its application in various fields such as design of energy absorption devices or car or ship crushing. The basic folding mechanism model constructed and presented in Ref. [15] constitutes the basis for the calculation of the crushing strength of boxes or square tubes and the quasi-static cross section methods used for determination of ship bow response. Modelling involving axial crushing of circular tubes can be found in Refs. [16] and [17]. The plastic energy can be evaluated from the axial deformation of the crushed tube in the form of a 'concertina', being equivalent to the work required to crush the element through a distance $2H$, where H is the distance between two plastic hinges of a convolution (Fig. 2).

In Ref. [18] the collapse modes are studied for convolutions formed internally. The dissipated plastic strain energy can be calculated [18] as:

$$E_b = 4\pi M_y \left(\frac{\pi D}{2} + H\right) \tag{7}$$

or from Refs. [19], as:

$$E_b = 2\pi\sigma_y t H^2 \left(1 + \frac{2}{3}\cdot\frac{H}{D}\right) \tag{8}$$

The above equations for the estimation of plastic energy absorption in the installation frame are applicable to braces adjacent to the struck legs or to the case with joint impacts in which the brace

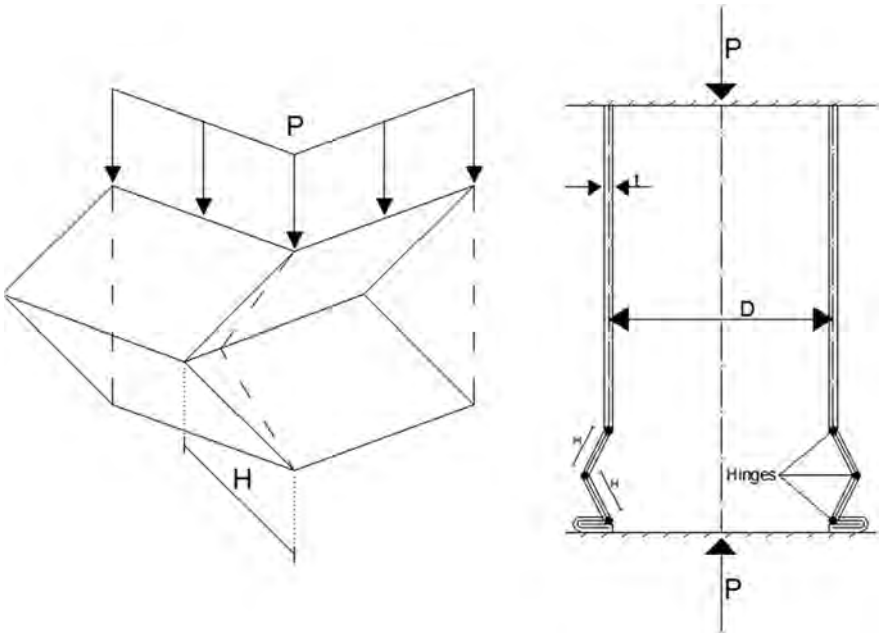

Fig. 2. Axial crushing mechanisms.

axial strength is lower than the leg transverse strength. However, for eccentric axial loads or long tube length, buckling of the platform tubes are more likely to exhibit modes similar to Euler buckling modes or even higher dynamic modes (Fig. 3) that lead to less amounts of energy absorption than those obtained for progressive buckling in Equations (7) and (8). Studies regarding transition from buckling to bending can be found in Refs. [20–24]. The energy absorbed during the development of an axisymmetric fold in, for instance, a brace can be estimated by Ref. [23]:

$$E_b = 2\pi\sigma_y t \cdot \left\{ t\left(\frac{\pi D}{2} + \tilde{l}\right) \Big/ \sqrt{3} + \tilde{l}^2 \right\} \tag{9}$$

where

$$\tilde{l} = \left(\frac{\pi D t}{2\sqrt{3}}\right)^{1/2} \tag{10}$$

Equation (9) is nevertheless only recommended for circular tubes with ratios $D/t \leq 40–45$ for being believed to underestimate the energy absorption for thicker tubes. This owes to the neglecting of the strain hardening effects and the absorption of some energy in axial compression at the development of each fold.

A parameter that also appears to influence the tube deformation under dynamic axial actions, besides its geometry, is the impact velocity of a striker [23]. From both experimental and numerical studies it is shown that the global bending mode develops quicker than progressive collapse for lower impact velocities, which can result in global bending of the tube, whereas higher impact velocities cause local folds (Fig. 3) to develop more rapidly than a global bending mode. It is possible that both the global bending and buckling modes are combined during the tube deformation under

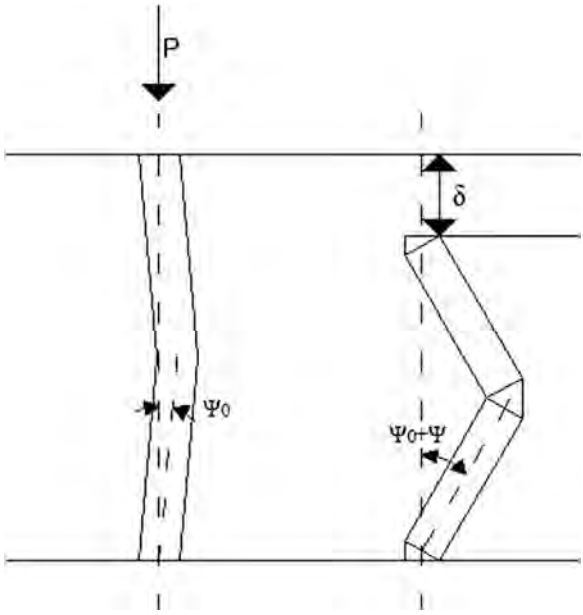

Fig. 3. Tube buckling.

compressive loading. The expressions currently known are thus not able to provide more than a general idea of the relative amounts of energy absorption by braces under compression in comparison with other deformation modes that the offshore facility is subjected to during the ship impact.

3. Ship loading

3.1. Ship types

According to [25] the number of world's cargo carrying fleet of propelled sea-going merchant ships of no less than 100 gross ton was estimated (in January 2013) to be 86,942, consisting of general cargo ships, tankers, bulk carriers, passenger ships, container ships and others. Among them, general cargo ships have the highest portion, and the oil tankers rank the second. Not only the sizes and layouts vary in these ships, but also steels of different strengths can be employed in shipbuilding. Therefore it is important to select more representative ship structures in the study as it is not possible to model all the ships. The International Association of Classification Societies (IACS) consisting of thirteen classification societies keep data of the majority of the world's cargo carrying ships' tonnage. From the number distributions of the principal general cargo ships, bulk cargo carriers, container ships, and oil tankers, analysed by the Systems Laboratory of Port and Harbour Research Institute (PHRI), the relationship between the vessel displacement *DT* and deadweight tonnage *DWT* can be established. Likewise, approximate relationships between the deadweight tonnage *DWT* and general dimensions (length − L_{pp}) can also be established as [26]:

$$\left.\begin{array}{l}\text{Cargo ships}(<10,000\text{DWT}) : \log(L_{pp}) = 0.867 + 0.310\log(\text{DWT})\\ \text{Cargo ships}(\geq 10,000\text{DWT}) : \log(L_{pp}) = 0.964 + 0.285\log(\text{DWT})\\ \text{Container ships} : \log(L_{pp}) = 0.516 + 0.401\log(\text{DWT})\\ \text{Oil tankers} : \log(L_{pp}) = 0.793 + 0.322\log(\text{DWT})\end{array}\right\} \quad (11)$$

With regards to collision assessment of ships with offshore installations, the DNV design against accidental loads [3] prescribes deformation relationships for bows against jacket legs for supply vessels between 2000 and 5000 tons and energy impacts up to approximately 60 MJ, meaning, for instance, velocities of approximately 6 m/s for a vessel of ~3000 ton. Nonetheless, the trend observed in recent years is that heavier vessels have been being built. According to [27], vessel displacements have been increased since 1985—6000 tons and Central North Sea and Southern North Sea structures have been subjected to collisions involving vessels up to 10,000 tons. The supply vessel can also differ according to where it operates, ranging, for instance, from 1000 tons in the Gulf of Mexico to 8000 tons in the North Sea [4,5]. The nature of the collision events can also give an overview on how severe the facility damage can be. Different impact velocities are expected from regularly visiting supply vessels, passing vessels and off-loading shuttle tankers. Reports have shown [6] that the transfer of cargo followed by vessels that approach the installation and unloading operations seem to be the most common type of activities that lead to collisions with the offshore installation. Despite less frequent, incidents involving passing vessels have also been reported. These incidents involving passing vessels likely involve high energies from the impact caused by higher velocities, and the highest energy collisions are likely to involve head-on impacts.

Some models representing ships of different sizes have therefore been considered in this study. The fleet comprises the following models:

1) Ship 'S2' – for supply vessels with displacements between 2000 and 5000 tons when fully loaded;
2) Ship 'S10' – for heavier supply vessels. Stronger scantlings than usual are assumed for this model;
3) Ship 'S20' – greater than model 'S10', displacement up to about 25,000 ton;

The scantlings of these models are given in detail in the Appendix, whereas the particulars concerning the FEM are described in the next section.

3.2. FE models

Since the ship models have been chosen with the purpose of evaluating collisions that involve high amounts of energy, i.e., head on collisions, particular attention has been given to the ship bows. It is true that for lateral collision the hydrodynamic mass coefficients are greater than for bow impacts. However the velocities of head on collisions are higher, therefore leading to higher impact energy. The modelling of ship striking bows in literature diverges from rigid and approximate shapes [28] to detailed models with the deformable structure represented [29,30]. Bows can be divided into conventional and bulbous. For the second case, the bow is expected to provoke higher stresses on the obstacle due to the increased stiffness resulting from the bulb contribution. In the current work the three ships are modelled with bulbous bows. Decks, frames and girders are included in all the models. The influence of longitudinal stiffeners is also checked by comparing the simulation results obtained with or without including the stiffeners in the model. Two other parameters which influence the bow deformation response are also considered. They are the strength of the scantlings and steel types. For the first, the scantlings are increased by increasing the thickness of the plates, while for the second different stress–strain curves are assumed. Some attention is also put on the impact velocity and the width of the obstacle, i.e., the contact area between the struck object and the striking bow.

The stress–strain curves of the ship steels used in the simulations meet the IACS criteria and are obtained from tensile tests [31]. The steels for scantling purposes have usually minimum yield stresses ranging from 235 MPa to 390 MPa (oil tankers and bulk carriers). In this study yield stresses of 285 MPa and 365 MPa are considered for mild steel and high strength steel, and named as 'M' and 'HT' respectively. The curves of the piecewise linear plasticity material models adopted in the simulations and remaining mechanical properties are shown in Fig. 4 and Table 1. Strain rate values are defined according to [32] and [33] for the different steel types and the Cowper-Symonds (standard strain rate formulation) model is used [34]. The critical fracture strain values are set according to the element size of the adopted mesh size and the nominal values normally taken for steel materials, usually assumed

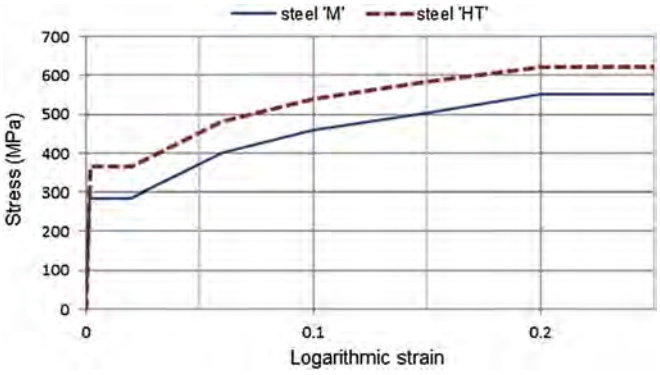

Fig. 4. Stress-strain curves of ship steels.

between 0.15 and 0.2 [3]. Shell elements of size between 80 mm and 100 mm are used for the steel plates of first sections of the ship. The element size is determined after performing mesh convergence tests [14,35,36]. Due to the variation of plate thickness for different ship models the range of ε_u may also vary. The fracture of the steel is of some importance in modelling the bow crushing behaviour as it can affect the bow secondary stiffness, i.e. the restore of the ship strength during the internal contact between different plates from the ship structure. For the rear part of the ships, where no significant deformations are expected to occur, rigid solid elements are employed and rigidly connected to the shells of the front portion. The total mass of the ships is obtained by adjusting the density of the rigid blocks, and the ships real shape is kept in order to capture the inertia effects in the model and to model the right gyration radii. A constant value for the surge added mass has been assumed knowing that, however, in a few cases some yawing can develop during the slowing down process and also the kinetic energy might not reach zero. The total mass of the models also includes the hydrodynamic added mass of 5–10% assumed for surge.

3.3. Bow deformation

The estimation of the deformation and loading exerted by striking bows has been addressed, since Minorsky [37], either via mathematical models [32,38,39], or model tests [40–42]. The mathematical models have been developed from the basic folding mechanisms [43] described in Section 2 (Fig. 2) and continuously improved. In general, for such quasi-static analysis it is required that the ship layout/structure susceptible of deformation is well known as the deformations are evaluated based upon the number and nature of the plate intersections in each cross section along the ship length. This might turn such procedures too complex as part of the full collision analysis of vessels against offshore facilities.

Because a very high level of detail could be, to some extent, very time consuming, not only in terms of the model complexity, but also by means of FE calculation time, the concept of equivalent plate

Table 1
Steel properties of the ship models.

Steel type	E [GPa]	σ_y [MPa]	σ_u [MPa]	ε_u	$\sqrt{}$	ρ [Kg/m^3]	C [s^{-1}]	P
'M'	200	285	550	0.17–0.37[a]	0.3	7800 [32]	500 [32]	4
'HT'	200	365	620	0.17–0.37[a]	0.3	7800 [33]	3200 [33]	5

[a] Dependent on the shell thickness.

thickness [44] could be plausible in order to account for the effects of relatively small stiffeners. In this case, the stiffened bow is replaced by an unstiffened structure in which the outer shell is calculated, following the smearing out technique as:

$$t_{eq} = t + k\frac{A_s}{\delta} \tag{12}$$

where t_{eq} is the equivalent thickness, t is the thickness of the outer shell, k is an empirical constant usually taken as 1.0, A_s stands for the sectional area of the stiffeners and δ represents the spacing between the stiffeners. Experiments by Paik and Pedersen [45] have shown that longitudinally stiffened structures could be reasonably replaced by equivalent unstiffened structures by using the smearing out technique (Fig. 5). This method was applied by Yamada and Pedersen [46] in combination with Yang and Caldwell's method [32] to different kinds of bulbous sections. In fact, the mean crushing forces calculated for the equivalent unstiffened structure are lower, although they could be more accurate when correlated with experimental data. The neglecting of lateral buckling of the stiffeners actually results in a lower value of the plastic bending moment M_0. The adopted technique is considered for the assumed striking bows with moderate deformations since for a struck ship, the fracture initiation could take place at a different location than the ship front.

Simple empirical formulae have been derived by other authors, making use of databases of previous collision cases and other statistical data. Parameters such as the ship total mass, ship size, impact velocity, strain rate effects are accounted in different expressions. Saul and Svensson [47] give the maximum impact force based on the deadweight of the vessel with a scatter of 50% based on the bow shape and structure type:

$$P_{bow}[\mathrm{MN}] = 0.88\sqrt{\mathrm{DWT}} \pm 50\% \tag{13}$$

The US-Guide Specifications [48] estimate the maximum crushing force with the inclusion of the ship initial velocity v_0 by:

$$P_{bow}[\mathrm{MN}] = 0.12 v_0 \sqrt{\mathrm{DWT}} \tag{14}$$

while Pedersen [49] derived an empirical expression, for ice-strengthened bows, based on a series of analysed collision cases using Amdahl's [39] and Caldwell and Yang's [32] procedures, for the calculation of the maximum bow collision load that also takes into account the ship length L_{pp}:

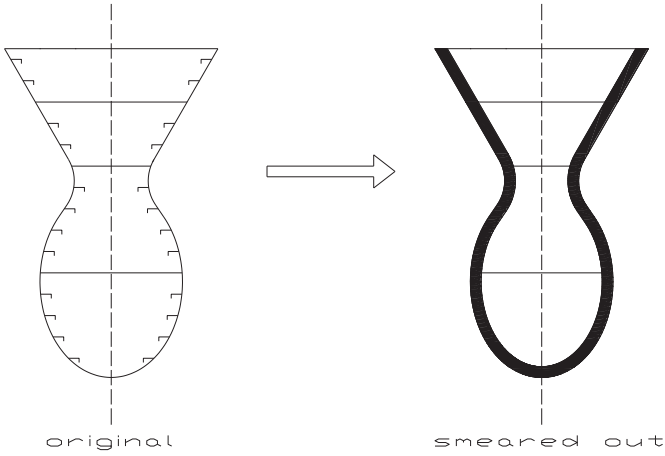

Fig. 5. Stiffened bow section vs. unstiffened bow section with smeared out thickness.

$$P_{\text{bow}}[\text{MN}] = \begin{cases} 210 \cdot \bar{L}\left[\bar{E}_{\text{bow}} + (5.0 - \bar{L})\bar{L}^{1.6}\right]^{0.5} & \Rightarrow \bar{E}_{\text{bow}} \geq \bar{L}^{2.6} \\ 470.4 \cdot P_0 \left[\bar{E}_{\text{bow}}\bar{L}\right]^{0.5} & \Rightarrow \bar{E}_{\text{bow}} < \bar{L}^{2.6} \end{cases} \tag{15}$$

where

$$\bar{L} = L_{pp}/275\ [\text{m}];$$

$$\bar{E}_{\text{bow}} = E_{bow}/1425\ [\text{MJ}];$$

$$E_{\text{bow}} = 1/2 \cdot 1.05 \cdot m_{\text{ship}} \cdot v_0^2\ [\text{MJ}].$$

It is however common to all these expressions that the width of the struck obstacle is neglected, and thus the bow response for impacts against obstacles of limited width would likely overestimate the deformed steel volume and underestimate the penetration depth of the obstacle. The eccentricity for impacts against obstacles of limited width is another parameter that must be taken into account, not only due to the different strength of the contact areas between ship and obstacle, but also because of the hydrodynamic effects.

To account for all the above issues, in this study numerical simulations are carried out first by subjecting the three bow models against rigid obstacles.

Despite the impact velocity is considered in some of the above formulae, it is shown in Fig. 6, from the impact forces calculated according to Equation (13), that its influence is not noticeable on the bow deformation caused by a fixed rigid object, in which the force-deformation curves for different velocities are obtained for Ship 'S10' using steel 'M' and larger scantlings against a rigid cylinder of $D = 2$ m. For initial velocities of 3, 5 and 7 m/s the contact force can be directly related to the crushing distance (s) since it is mainly a function of the amount of kinetic energy.

The comparison between the deformation of the same ship model using the stiffened bow and unstiffened bow with smeared out thickness is also made for an impact speed of 7 m/s (Fig. 7), where the reduction of the bow force with the crushing distance can be about 10%–20% for penetration depths greater than 2 m. The same bow is considered with the same impact speed against a rigid wall, which shows an increase of the peak force from 81.7 MN to 96.9 MN (19% increase) and a decrease of

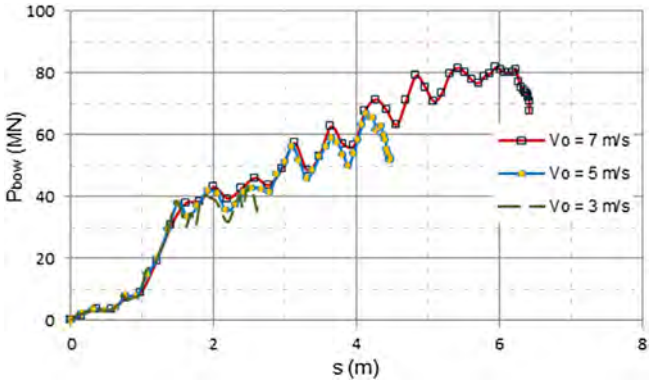

Fig. 6. Bow deformation for different impact velocities (ship 'S10').

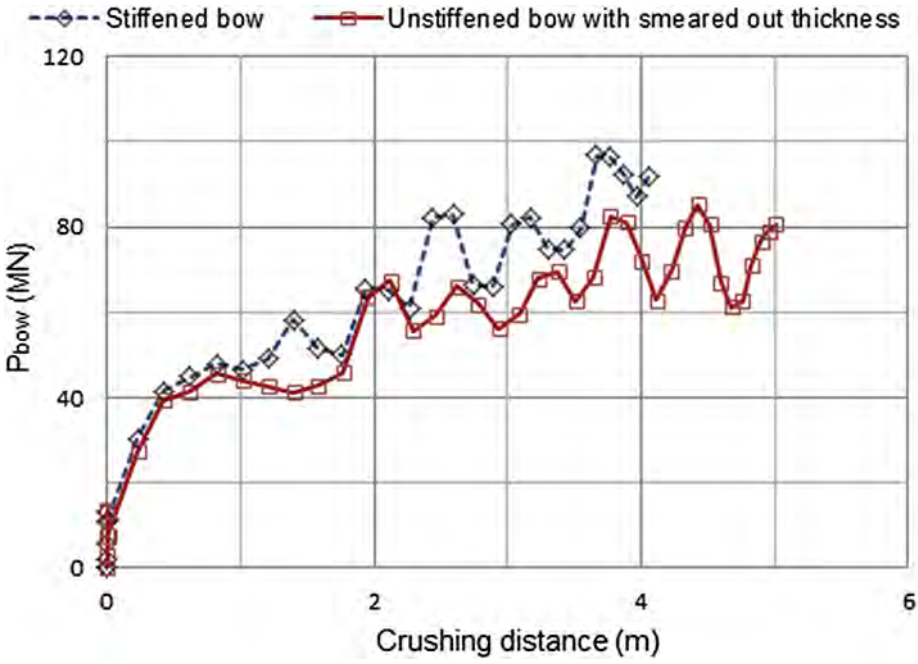

Fig. 7. Stiffened bow section vs. unstiffened bow section with smeared out thickness (ship 'S10' vs. rigid wall).

the bow crushing distance from 6.4 m to 4.7 m (27% decrease) relatively to the impact with the rigid cylinder (bow deformation illustrated in Fig. 8). This proves the importance of accounting for the width of the struck obstacles, especially when evaluation of the energy dissipation is based upon the stiffness of the contact areas.

The influences of other parameters such as different scantlings and steel materials are examined for the three bow models against a rigid cylinder of 2.0 m diameter (Fig. 9) and are compared with the predictions from other authors in Fig. 10. The classification of the ships, according to their deadweight

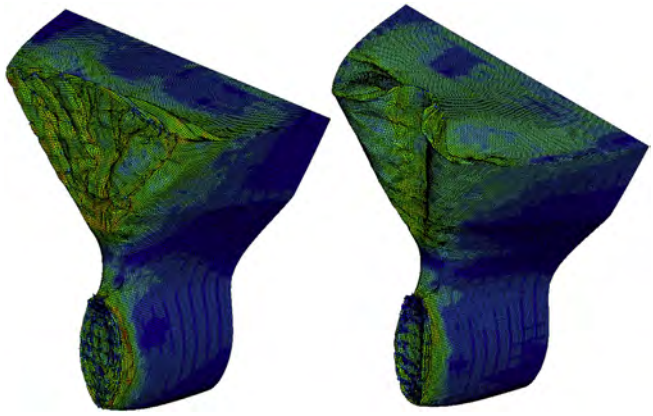

Fig. 8. Bow deformation, stiffened model 'S10' (left – rigid wall; right – rigid cylinder).

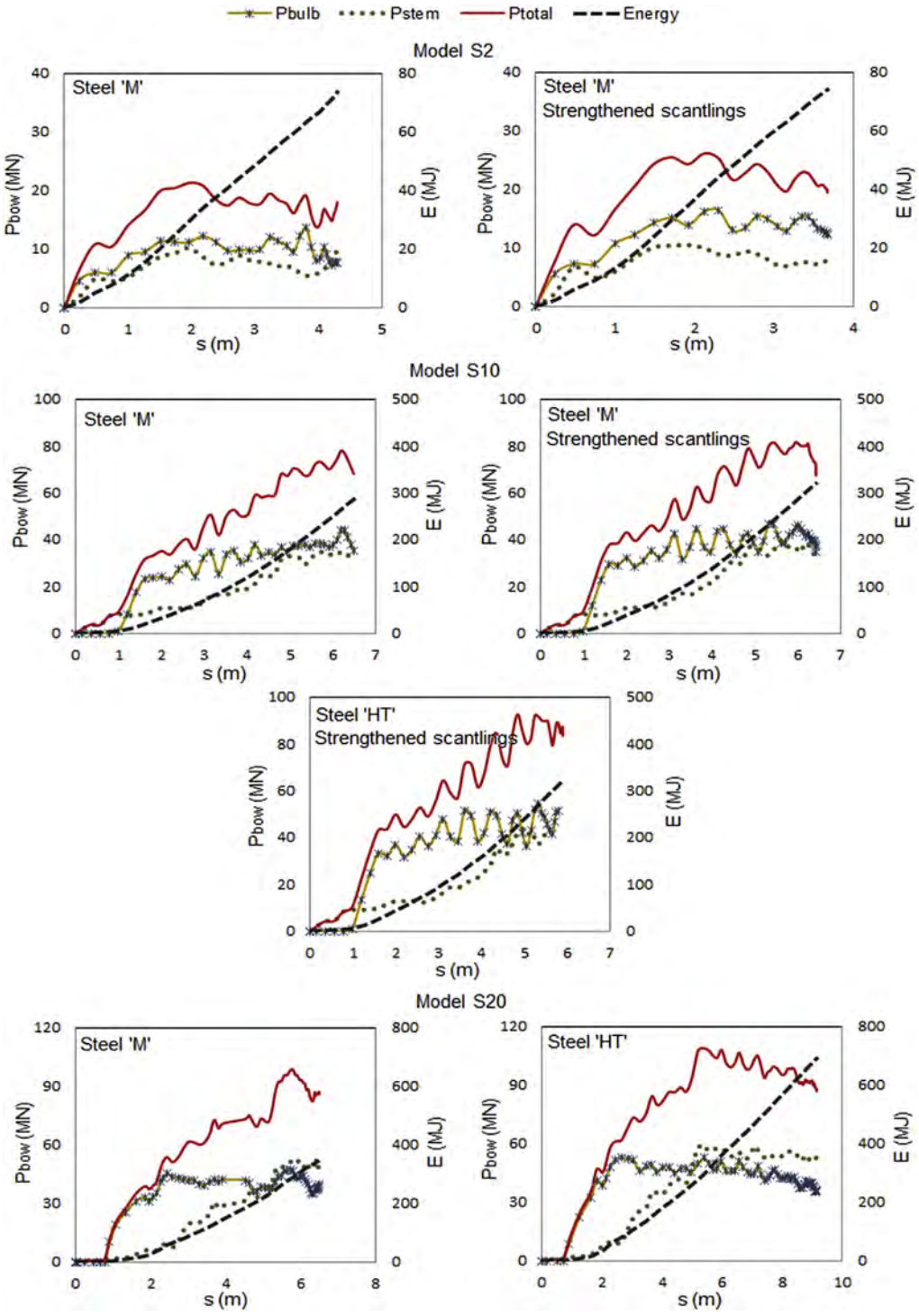

Fig. 9. Bow deformation (FEA).

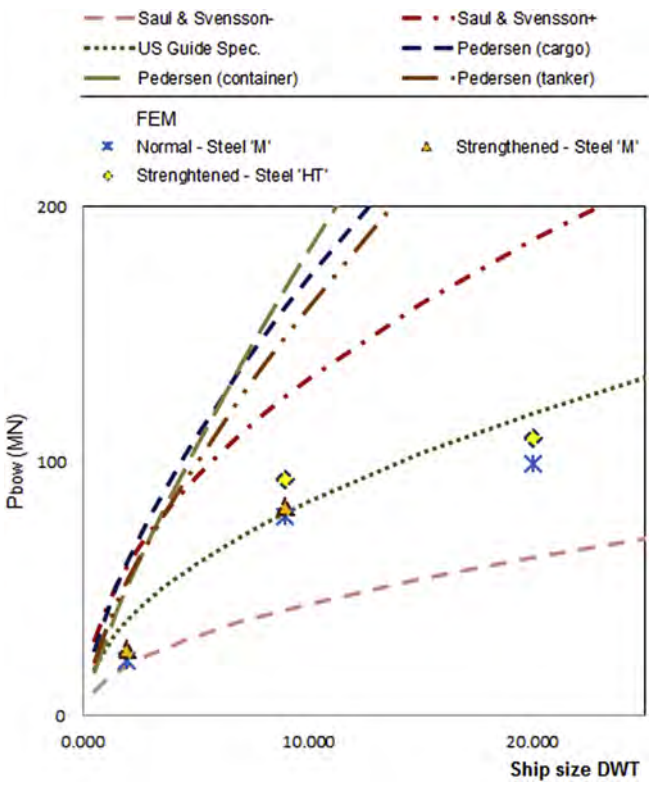

Fig. 10. Bow maximum forces.

tonnage, is made according to the statistical data from Refs. [26], as well as considering Equation (13) in order to estimate the bow forces according to [49]. The penetration depth s is obtained/measured from the forecastle deck end that can be more or less forward in comparison with the bulb, depending on the different bow configurations.

The difference between the various predictions confirms the difficulty in generalizing the deformation response of ship bows, especially if accounting for special ship categories or by looking at both upper and lower bounds of Equation (13). However, regardless of the variations of the rigid obstacle width or the bow layout (stiffened or unstiffened with smeared out thickness), the FEA seem to show good agreement with the curve from the US Guide (Equation (14)), and is in between the upper and lower bounds from Saul & Svensson's curve (Equation (13)). Equation (15) clearly indicates greater bow forces and the respective spread of them.

3.4. Simplified equivalent system

Knowing that explicit finite-element techniques may not be ideal for practical engineering problems, as the explicit integration of the models normally requires supercomputing resources and long calculation time, simplified systems are developed for efficient bow crushing response analysis, based on the FEA. By assuming that in a frontal collision the energy absorbed is mainly function of the deformation in the direction of the initial ship motion (surge), the deformed bow can be replaced by a spring (SDOF) or a set of springs in parallel. In Ref. [50], where the bow deformation is studied for ship–ship collisions, the calculations of the collision damage consider

the vertical variation in the stiffness of the striking bow. The bow stiffness is then represented as a set of non-linear springs modelled according to [51] with associated slacks representing the geometrical bow form. From observing the energy curves in Fig. 6, it can be drawn that their growth follows a quadratic trend (at least) until the peak force is reached. After that point, the increase is nearly linear with the null growth of the contact force. The energy curves for the ascending trend of the force can therefore be approximated as:

$$E_{\text{bow}} = A \cdot s^2 + B \cdot s \tag{16}$$

and the force obtained from:

$$P_{\text{bow}} = \frac{\partial E_{\text{bow}}}{\partial s} = \kappa \cdot s + B \tag{17}$$

where A and B are constants that characterize the force and energy curves and $\kappa = 2A$.The spring law is then described by a rigid behaviour until the force reaches a magnitude of B. From this point until reaching the peak force, the spring deforms linearly with a stiffness value equal to κ. Such parameters might also provide a practical tool in evaluating the energy dissipation based on the relative stiffness approach when the struck obstacles are deformable too.

When it comes to collisions in which the bow is only partially involved, a simplified system using two or more springs in parallel may reproduce the ship response more accurately. This is the case, for instance, when the obstacle is an inclined platform leg or even a brace. The curves in Fig. 6 are plotted assuming two parts of typical bulbous bows of which loading on a struck obstacle could be split into two main and distinct highly concentrated stress areas from bulb and stem (Fig. 11).

The bows under analysis have higher strength when compared to conventional bows due to the inclusion of the bulb in the structure, which is also the stiffer part of the bow. Based on the FEA, the trends shown in Fig. 12 are assumed for estimation of κ and B from the ship dimensions, including factors such as the strength of the scantlings and the steel grades. Since the evaluation is carried out considering central deformations, for eccentric impacts both loading and κ and B would be lower if the contact parts did not involve the central girders. For eccentric impacts the ship would likely rotate over the obstacle, therefore changing the direction of the penetration and the hydrodynamic mass factors would equally have to be readjusted due to the ship sway. Another consideration to be done with regards to the stiffness of the springs used in the equivalent systems is that after the maximum contact load the bow force seems either to reach a plateau or decrease. Thus, in case of a very stiff obstacle penetrating the ship bow much further than the limits

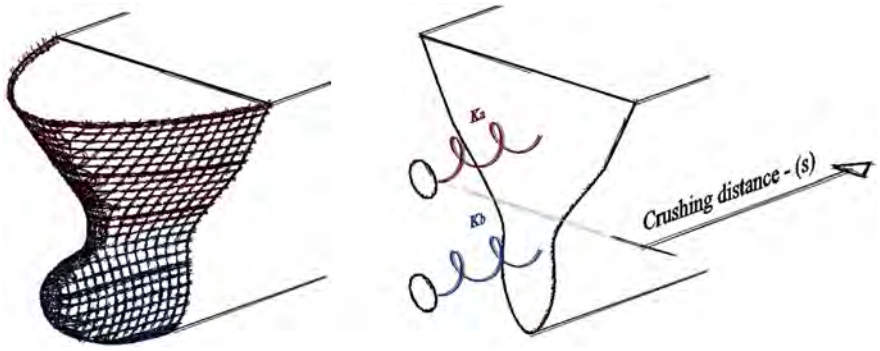

Fig. 11. Simplified system for bow response.

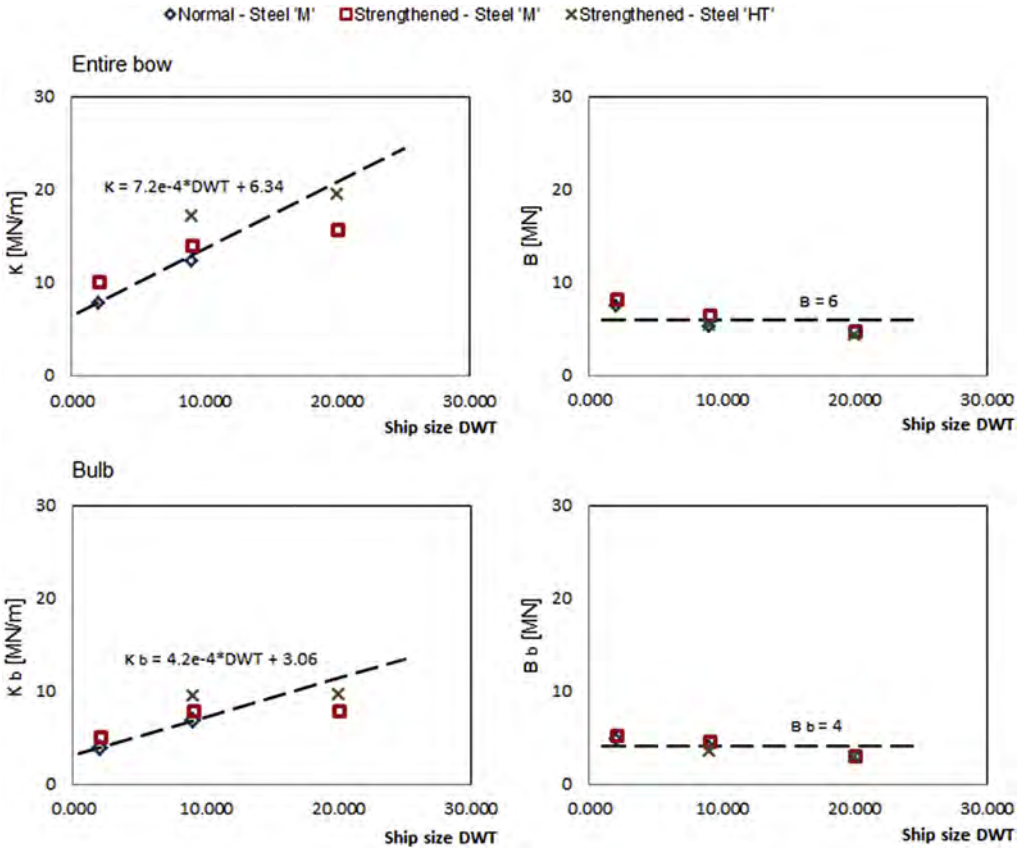

Fig. 12. Estimation of simplified ship bow equivalent system.

considered in the analysis (higher energy impacts) the spring stiffness shall rather be considered as null after the penetration depth corresponding to the maximum force has been reached. Values for κ and B are also given if only the bulb is accounted/involved during the collision (κ_b and B_b). The same can be estimated for the remaining part separately from the idealization of a system of parallel springs (κ_a and B_a).

The curve fit for κ in Fig. 12 is done for the three different bow models considering the respective variations in terms of plate thickness or steel strength. For model 'S20' the shell thickness of the unstiffened bow is smeared out, making κ to lie below the projection. It has already been shown for model 'S10' that for equal crushing depths the difference between the peak force using stiffened and unstiffened bows with increased shell thickness varies between 10 and 20%. The respective equivalent spring stiffness is therefore affected. The use of larger scantlings that can be more representative of special ship classes could also indicate the projections to be conservative for the majority of the cases as these ICE class ships or similar are less common. As for parameter B, it appears that the reference value of the force for which bow deformations start to become significant should be taken as constant regardless of the ship size (if within the range of the vessel sizes considered). Yet, the extrapolation of these values for ships of possible higher impact energies is not recommended and does not seem to be of significant interest as the respective strengths and energy amounts for collisions involving such vessels would likely go much beyond the order of magnitude that offshore steel fixed platforms could bear.

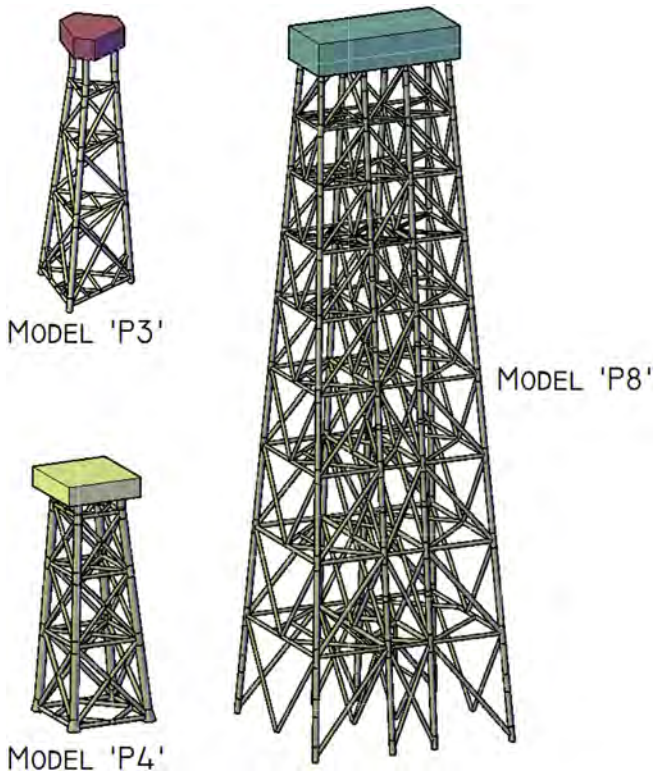

Fig. 13. Offshore platform models.

4. Collision simulations

4.1. Platform models

For the purpose of examining the energy dissipations on different strength obstacles, three platform models are considered: a tripod, 'P3', and a four-legged jacket, 'P4', with the total heights from the seabed to the deck of 71.0 m and 53.6 m, respectively; and an eight-legged jacket model, 'P8', for deeper waters with a height of 201.2 m (Fig. 13). The steel frames of the three platforms are constituted by tubular members, with the material properties described in Table 2. The API RP-2A [22] requires that structural steel pipes must conform to the American Society for Testing and Materials (ASTM) A36, with yield strength of around 250 MPa. However, the medium grade structural steels of which offshore platforms are conventionally constructed have yield strengths in the range of 350 MPa with some platforms installed in the North Sea having been constructed with 400–450 MPa steel, according to [52]. The joints are modelled as welded in this study. For different collision cases the same platform model is given different thickness values so that not only global but mainly local strength and different ship/platform stiffness ratios could be considered in the

Table 2
Platforms steel material.

Part description	E [GPa]	σ_y [MPa]	σ_u [MPa]	ε_u	$\sqrt{}$	ρ [Kg/m^3]	C [s^{-1}]	P
Tube	200	345	450	0.20	0.3	7800	40.4 [34]	5 [34]

evaluation of energy dissipation. Impacted legs have lengths ranging between ~15 and ~25 m and diameters of 1.25–1.70 m, whereas the struck braces range in length from ~14.0 m to 20.0 m and have diameters of 0.5 m and 0.8 m. The steel frames of models 'P3' and 'P4' are discretised with shell elements, while for model 'P8' only the two top storeys (see Appendix) are modelled using shells. Due to the dimensions and complexity of the model 'P8' and in order to save computation resources, the rest of the frame where no big plastic deformations are expected from the impact, beam elements are used. The fracture strain for the defined steel materials is adjusted according to the mesh size of the shell elements (100 mm) and thickness. The mesh size is determined after a mesh convergence test. The top decks of the platforms are rigidly connected to the frames and modelled using rigid materials. The vertical action of gravity is added to the deck and the design weight values adopted are checked according to the axial preload design values [5]. The mass values are 8000, 10,000 and 12,500 ton for models 'P3', 'P4' and 'P8' respectively. The structural particulars of the platform models can be seen more in detail in the Appendix.

4.2. Collision cases

The numerical models for ships and platforms described above are used to perform ship collision simulations. The case studies under analysis refer to different possibilities of ship-platform collision and different deformation scenarios. As mentioned earlier, not only different ship and platform models are used, but also the strength of some of the tubular steel members is adjusted by changing the thickness. It is expected that by adjusting the relative thickness of ship and installation the energy may be dissipated through the different structures in different proportions and also through the different plastic mechanisms formed. The collision scenarios are illustrated in Fig. 14 and the initial data reporting to each collision case are shown in Table 3. The scenarios considered include collisions on leg, joint and brace as well as different impact angles. The position of the arrows in Fig. 14 indicates the approximate position of the highest concentrated stresses caused by the contact. This should normally correspond to the bulb position. The only exception is case 19, in which the upper part of the bow strikes the brace. In case 20 the contact also involves the struck brace of case 19 although the ship position is lowered. For reasons of simplification and analysis, the same thickness values indicated in Table 3 are used for all the braces or legs.

4.3. Model response

Unless the offshore steel frames have very stiff elements as well as stiff connections and stronger bracings, the energies involved in any of the scenarios should be enough to provoke the individual

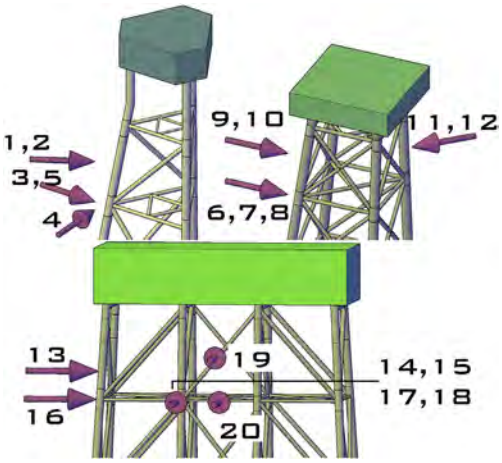

Fig. 14. Collision scenarios.

Table 3
Description of collision cases.

Case	Ship					Installation		
	Model	Scantlings	Steel	v_0 m/s	E_{k0} MJ	Model	t_{leg} [mm]	t_{brace} [mm]
1	'S2'	Normal	'M'	7.0	74.3	'P3'	60	20
2	'S2'	Normal	'M'	7.0	74.3	'P3'	45	20
3	'S2'	Normal	'M'	7.0	74.3	'P3'	60	20
4	'S2'	Normal	'M'	7.0	74.3	'P3'	60	20
5	'S2'	Normal	'M'	7.0	74.3	'P3'	45	20
6	'S2'	Normal	'M'	6.0	54.6	'P4'	60	20
7	'S2'	Normal	'M'	6.0	54.6	'P4'	45	20
8	'S10'	Large	'M'	3.0	59.0	'P4'	60	20
9	'S2'	Normal	'M'	6.0	54.6	'P4'	60	20
10	'S2'	Normal	'M'	6.0	54.6	'P4'	45	20
11	'S2'	Normal	'M'	6.0	54.6	'P4'	60	20
12	'S2'	Normal	'M'	6.0	54.6	'P4'	45	20
13	'S2'	Large	'M'	7.0	74.4	'P8'	50	15
14	'S2'	Large	'M'	7.0	74.4	'P8'	50	15
15	'S2'	Large	'M'	7.0	74.4	'P8'	70	20
16	'S10'	Large	'M'	4.0	104.8	'P8'	50	15
17	'S10'	Large	'M'	4.0	104.8	'P8'	50	15
18	'S10'	Large	'M'	4.0	104.8	'P8'	50	20
19	'S2'	Large	'M'	4.0	24.3	'P8'	50	20
20	'S2'	Large	'M'	4.0	24.3	'P8'	50	20

failure of some members. The need of considering higher redundant platforms such as model 'P8' owes to a better assessment of the contribution from different plastic mechanisms in the whole system (vessel + installation) response. For instance, in cases 2 and 5, the deck of platform 'P3' falls (global collapse of the deck) after the failure of the hit leg, regardless of the impact type – beam or joint. The amounts of internal energy of the installation are in both cases similar (see Table 4), but the failure

Table 4
Energy balance.

Case	Total energy							Strain energy		
	E_{ship} [MJ]	E_{ship} [%]	E_{inst} [MJ]	E_{inst} [%]	$E_{rebound}$ [MJ]	$E_{rebound}$ [%]	E_{total} [MJ]	E_{ship} [%]	E_{inst} [%]	E_{total} [MJ]
1	69.0	92.9	4.2	5.6	1.1	1.5	74.3	94.3	5.7	73.2
2	36.5	49.1	28.7	38.6	9.2[a]	12.3[a]	74.3	56.0	44.0	65.2
3	61.9	83.2	11.5	15.4	1.0	1.3	74.3	84.4	15.6	73.3
4	64.9	87.3	7.7	10.3	1.8	2.4	74.3	89.4	10.6	72.6
5	37.7	50.7	27.5	37.0	9.1[a]	12.2[a]	74.3	57.8	42.2	65.2
6	50.3	92.2	3.3	6.0	1.0	1.8	54.6	93.9	6.1	53.6
7	47.8	87.6	5.7	10.4	1.1	2.0	54.6	89.4	10.6	53.5
8	34.3	58.2	8.1	13.7	16.6[a]	28.2[a]	59.0	81.0	19.0	42.4
9	49.1	90.0	4.2	7.8	1.2	2.3	54.6	92.1	7.9	53.4
10	46.3	84.8	6.9	12.6	1.4	2.6	54.6	87.1	12.9	53.2
11	52.2	95.7	1.5	2.7	0.9	1.7	54.6	97.3	2.7	53.7
12	50.3	92.1	3.1	5.7	1.2	2.2	54.6	94.2	5.8	53.4
13	63.0	84.6	11.0	14.8	0.4	0.6	74.4	85.1	14.9	74.0
14	32.6	43.8	40.6	54.5	1.2	1.7	74.4	44.6	55.4	73.2
15	48.1	64.7	25.7	34.6	0.6	0.7	74.4	65.2	34.8	73.9
16	34.6	33.0	68.8	65.6	1.4	1.3	104.8	33.5	66.5	103.4
17	32.8	31.3	71.5	64.0	4.9	4.7	104.8	32.9	67.1	104.3
18	55.6	53.0	49.2	46.9	0.0	0.0	104.8	53.0	47.0	104.8
19	0.2	0.8	7.9	32.5[b]	16.2	66.7[b]	24.3	2.5	97.5	8.1
20	2.0	8.2	16.2	66.7[b]	6.1	25.1[b]	24.3	11.0	89.0	18.2

[a] Deck fall.
[b] Brace failure.

mechanisms are highly influenced by the gravity action on the deck after the global collapse has occurred. In fact, the platform has absorbed respectively 11.2 MJ and 12.3 MJ energy when the leg failure occurs. In contrast, for platform 'P8', larger dents on the leg wall and eventual leg fracture are not sufficient to lead to an overall structural collapse. The energy dissipation in each of the numerical cases is shown in Table 4 and in Table 5 the platform response is described more in detail, considering the different deformation mechanisms.

Attention must be paid to any connection that can be made between the displacement of the membrane of the hit zone of the tube platform and the energy dissipated. For situations in which the full leg is able to bend without any local denting, the values u (displacement of the struck membrane of the platform due to beam bending, local denting or both) and Δ (displacement of the rigid deck) can be directly correlated with the configuration of the structure shape due to the impact action and respective wave propagation through the frame. This is actually regarded in cases 4 and 13, where the strain energy is assumed as part of the overall strain energy. In general, the values of the strain energy can also be well estimated using Equation (1) if u as given in Table 5 is relatively small as compared to the tube diameter.

The contribution of adjacent braces near the contact point is visible especially when the platforms are single or K-braced ('P3' and 'P8'). The strain energy absorbed by each of the braces in which the plastic deformations are significant is shown in Table 6 (u_b stands for the maximum deformation measured perpendicular to the tube axis due to axial compression) and Fig. 15. The relationship between the deformation configuration and the amount of strain energy of the braces due to axial compression is not of easy estimation since the development of folding can be combined with global bending. The maximum energy amounts on each of the braces subjected to axial actions are generally close and seem to vary more with the change of wall thickness rather than the diameter. As a reference, according to Equation (9) a variation of tube wall thickness from 15 to 20 mm for the range of diameters considered (0.5–0.8 m) would result in a factor of approximately 1.6 times more energy to develop an axisymmetric folding. In cases 17 and 18 it is still possible to figure out that the rupture of two braces

Table 5
Installation response.

Case	Global (jacket elastic response)			Localized						Total
	Δ [m]	E [MJ]	E [%]	Struck leg/brace/joint			Adjacent members[c]			
				u [m]	E [MJ]	E [%]	No. members	E [MJ]	E [%]	E [MJ]
1	<0.1	4.2	100	<0.1	~0	0	0	~0	0	4.2
2	[a]	[a]	[a]	[a]	[a]	[a]	[a]	[a]	[a]	28.7
3	0.26	7.9	68.7	0.13	~0	0	1	3.6	31.3	11.5
4	<0.1	7.7	100	0.17	~0	0	0	~0	0	7.7
5	[a]	[a]	[a]	[a]	[a]	[a]	[a]	[a]	[a]	27.5
6	<0.1	3.3	100	<0.1	~0	0	0	~0	0	3.3
7	<0.1	5.2	91.2	0.20	0.5	8.8	0	~0	0	5.7
8	<0.1	5.3	65.4	0.14	2.7	33.3	0	~0	0	8.1
9	<0.1	4.2	100	<0.1	~0	0	0	~0	0	4.2
10	<0.1	3.5	50.7	0.46	3.3	47.8	0	~0	0	6.9
11	<0.1	1.5	100	<0.1	~0	0	0	~0	0	1.5
12	<0.1	1.0	32.3	0.18	2.1	67.7	0	~0	0	3.1
13	0.70	11.0	100	0.60	~0	0	0	~0	0	11.0
14	0.70	14.1	34.7	1.93	20.1	49.5	1	6.4	15.8	40.6
15	0.71	12.4	48.2	1.43	13.3	51.8	0	~0	0	25.7
16	1.10	25.5	37.1	3.70	35.1	51.0	5	8.2	11.9	68.8
17	1.10	21.7	30.3	3.36	34.7	48.5	3	10.6	14.8	71.5
18	0.94	22.3	45.3	1.76	14.6	29.7	2	12.4	25.2	49.2
19	0.08	2.0	25.3	[b]	5.9	74.7	[b]	[b]	[b]	7.9
20	0.18	6.4	39.5	[b]	9.8	60.5	[b]	[b]	[b]	16.2

[a] Structure global collapse – only total internal energy of installation provided.
[b] Brace failure.
[c] Braces with significant local contribution to the total internal energy of the installation.

Table 6
Brace deformation caused by axial loading.

Case	L [m]	D [m]	t [mm]	u_b [m]	E MJ
3	25.5	0.8	20	1.5	3.7
14	20.0	0.8	15	1.5	2.8
16	15.2	0.5	15	2.7	3.1
17	9.2	0.5	15	3.8	3.0
18	9.2	0.5	20	2.0	4.7
18	20.0	0.8	20	0.9	3.6

occurs at the joint also due to the influence of shear. Nonetheless, the tubes under axial compression always end up failing before energy values reaching around 3 MJ for $t = 15$ mm and below 4 MJ for $t = 20$ mm. The only exception is found for case 18, where the failure occurs at an energy value of 4.7 MJ, possibly due to a stiffer brace with short length, which makes the transition from progressive buckling to global bending more difficult and therefore increases the capability of absorbing energy of the tube.

The configuration of the braces is equally important to define the overall strength of the installation. From the cases involving platform 'P4', there is no yielding in any other members than the hit leg. Despite in some of the cases that some small local denting is noticed for the $t = 45$ mm legs, the majority of the kinetic energy is converted into strain energy via ship deformation, whereas among the small portion of strain energy converted to the platform, the majority is taken by the frame deformation.

The frame deformation (global elastic deflection of the entire jacket) capacity associated with large global displacement of the frame is very important because it can absorb large amount of impact energy, in particular for bigger installations such as model 'P8'. The frame global energy is not only dependent on the stiffness of the structure in the impact direction, but also proportional to the squared displacement Δ (assuming a SDOF analogy [53]). The comparison between cases 15 and 18 can be illustrative of it if both values of Δ and E are accounted. Any of these 'global' energy values measured for model 'P8' from cases 14 to 18 presented in Table 5 are above those currently considered by any design code. However, in any of the collision scenarios both braces and legs can be subjected to local deformations, so that the local strength must always be considered. Still in regards to the measured Δ displacements, the model 'P3' undergoes considerable rotation over one of its legs (case 3) so that in such situations the rotational stiffness plays an important role in the way how the energy is transferred through the facility frame.

The interaction between ship and installation for each of the cases can be seen in Fig. 16. The displacements u and s are measured from the main contact point. Although these graphics can give a general idea of the relative strength of each of the structures and the energy taken by each of them, the energy absorbed by adjacent braces is not directly reflected on the global deformation curves (cases 3 and 16 to 18, for instance, when compared to the amounts given by Tables 4 and 5). Comparatively to the values shown in Table 5, the maximum u plotted in Fig. 16 is sometimes higher as they represent

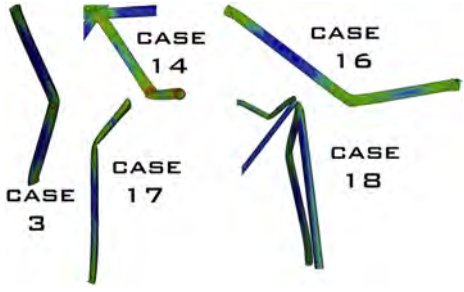

Fig. 15. Brace deformation due to axial compression.

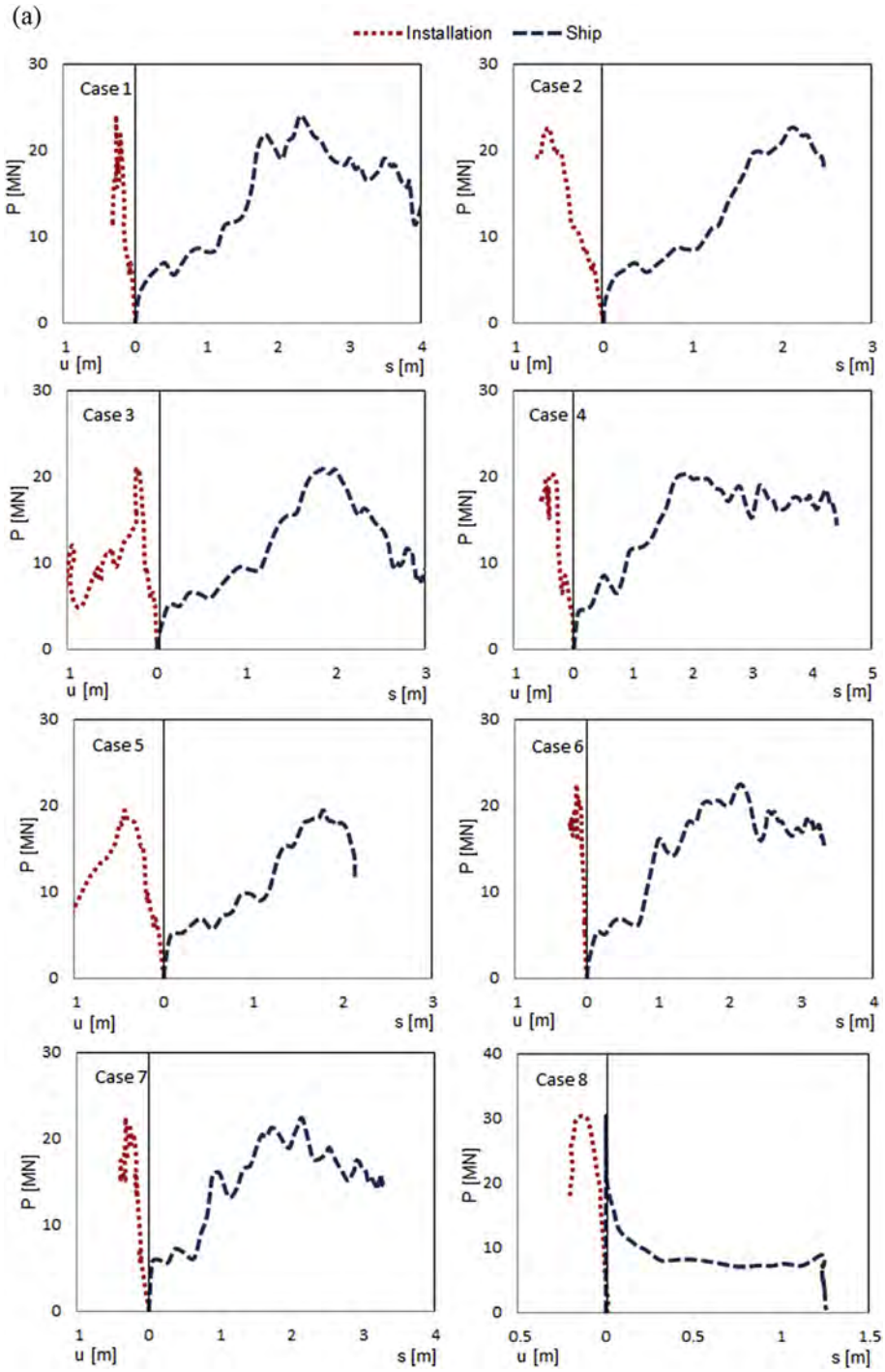

Fig. 16. a. Collision strain energy balance. b. Collision strain energy balance. c. Collision strain energy balance.

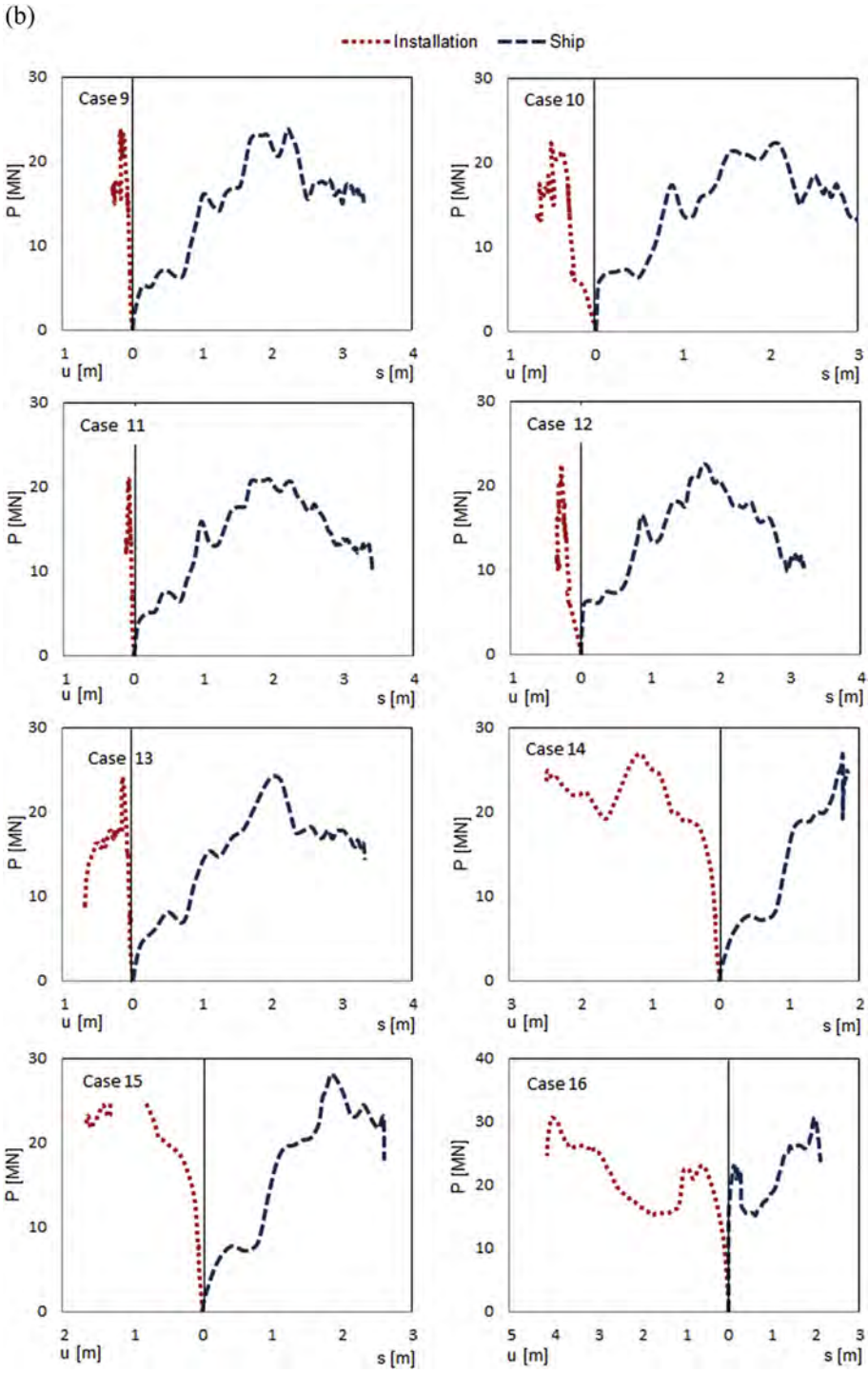

Fig. 16. (*continued*).

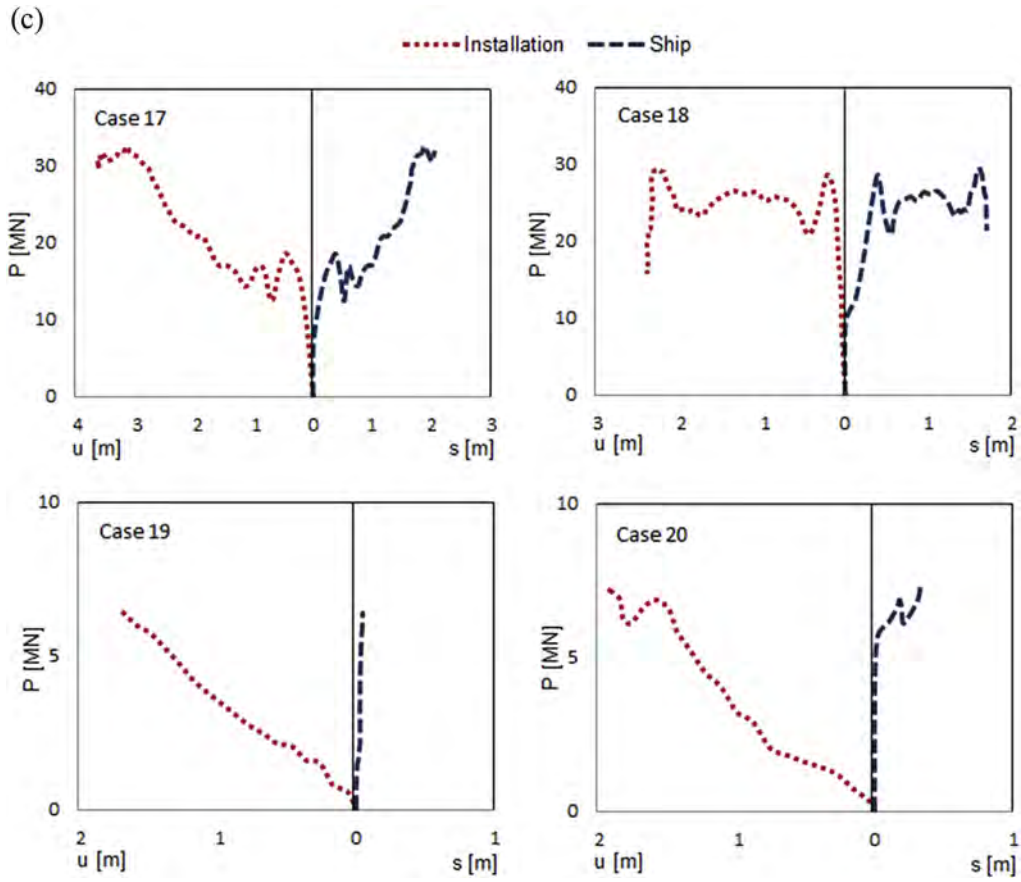

Fig. 16. (*continued*).

the peak values and not the final/residual displacements of Table 5 that account for the system unloading.

Another note concerns the way how the bow crushing distance must be pointed as in some cases, as mentioned earlier, the eccentricity of the collisions has to be considered and may influence the deformation configuration of the bow. Since it has been tried for all the situations that the ship bulb is aligned with the axis of the struck member and the global crushing distance *s* is measured from where the first deformations occur, these not always coincide with the centre of the ship at the forecastle deck (see Fig. 17). The approximated stiffness values estimated previously might therefore overestimate the ship action on the platform if simplified hand calculations are to be used.

5. Discussion

The set of numerical simulations described in the previous section provides meaningful information regarding the response of both ship and platform systems (and considering their interaction) within a range of diverse scenarios. The degree of complexity of these two structures demands the use of simplified equivalent systems for quick hand calculations. In both structures the formation of plastic mechanisms can involve various members. The development of numerical models for the estimation of the ship bow response is well documented and the bows can be assimilated to

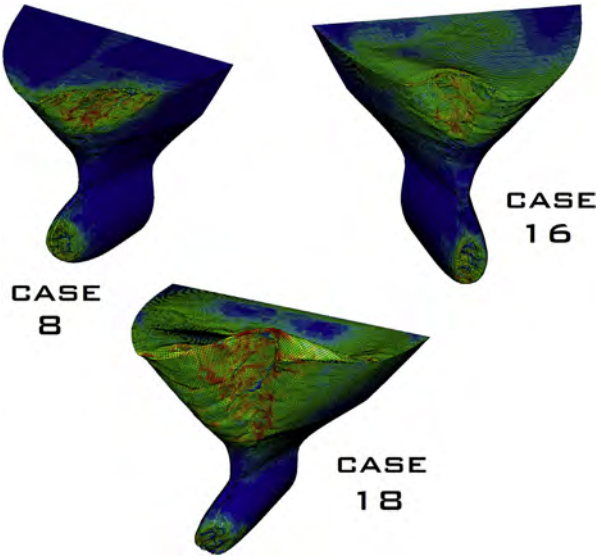

Fig. 17. Eccentric bow crushing.

a single or a small number of multiple degree of freedom systems. According to the calculations performed in Section 2, such models can be characterized mainly by springs initially rigid and then deformable according to an approximate constant plastic stiffness after the loading has reached a minimum value *B*. For the installation, although the deformation mechanisms of the members of the platform are normally assessed through simple hand calculations as well, adjacent members that are not directly involved in the collision can also experience significant deformations. This in fact makes the evaluation of the overall response more complex when such deformation mechanisms in different parts are combined. The separation between the different absorption mechanisms can become a complex process when taking into account the coupled response of both local and global effects. Whereas for beam impacts the mechanisms observed involve the flexural response of the struck member and the frame elastic response, provided that the connections are strong enough (for which the single bracings of case 3 is the only exception among the studied cases), when the ship action is directly exerted on a joint the adjacent braces are more likely to contribute to the formation of different mechanisms to the energy absorption process. Deformations caused by shear or axial crushing can be found for braces that are perpendicular or more aligned with the direction of the impact loading. Equations (7)–(10), however, cannot predict approximate energy amounts based on the deformations in braces, where these always differ from the illustrations of Figs. 2 and 3. This can make the estimation of the total response of the platform less accurate for joint impacts when the connections have a lower strength. For cases 14 and 16 to 18, of which deformed braces are shown in Fig. 15, different areas of concentrated stresses are noticeable for both ends and middle span. From the contribution/weight that the buckling of braces can have on the total response as shown in Table 5, the number of braces with plastic strain is shown to not necessarily reflect the total amount of energy taken by these members. Their contribution appears to reach up to approximately 25% of the total energy taken by the platform (collision 18), even though the separation between elastic and plastic strain energy is not made for the deformed tubes.

For the remaining cases where the flexural response of the struck leg or brace is responsible for the plastic strain energy of the installation, the analysis is easier to be carried out and the local mechanisms analysed in previous studies [7,8,13,14] can be employed effectively. As for the global energy, the frame elastic energy values given Table 5 follow the measured displacement Δ suggesting, for instance, the

use of simple SDOF analogies, provided that the global stiffness of the facility is not significantly affected by the local damage of the collision point [53].

With respect to the energy dissipation and respective design principles, a study by Storheim and Amdahl [54] takes into account the compactness factor R_c (Equations (1) and (5)) of the struck beam to predict the energy dissipation. The majority of the energy will be dissipated by the ship if R_c is larger than the maximum collision force, otherwise the platform member will deform according to a three-hinge-mechanism as described in Ref. [13]. In Ref. [54] values of $R_c > 1.7$ MN are assumed to be sufficient to crush the bulbous bows without significant denting ($R_c > 1.3$ MN for broadside impacts), according to the tube characteristics, the leg of 45–60 mm thickness, depending on the diameter. These values are obtained assuming a concentrated load, i.e. parameter b which is used in Ref. [3] for the tube resistance against local denting and in Equations (1)–(5) is equal to 0. If distributed loads from the contact area are considered then R_c could in theory assume lower values than those presented for $b = 0$.

For a consistent ship/installation stiffness ratio that can be practical in estimating the energy dissipation from collisions involving significant amounts of kinetic energy, it has been shown that different mechanisms and their interaction need to be addressed. For the ship structure, statistical data that account for parameters such as the plate thickness, ship dimensions or number of plate intersections are taken in order to derive SDOF or MDOF consisting of parallel springs, from which the spring stiffness can be derived. For the platform, however, the frame deformation is shown to dissipate high percentages of the total energy besides the local mechanisms occurred in or nearby the collision point. Expressions from Refs. [7,8] have a degree of ½, contrary to the quadratic equations derived for the deformation of the bow models. As for Equation (1), the complexity is higher since it depends on the relationship between the length of the dent and the diameter of the cross section. In turn, the stiffness assessment through beam bending or even the global displacement of the facility would mainly consider the linear response of the platform. For steel facilities like those considered in this study, i.e. made of tubular thin-walled members, the wall thickness plays an important role especially in how the local (and also global) strength is considered for purposes of comparison with the bow strength. The energy dissipation (strain energy, E) with respect to the relative strength is described in Fig. 18 for three different ratios/parameters. The three parameters taken into consideration for the installation are the stiffness obtained by the displacement measured on the impact point upon the application of a unit load κ_i, the compactness factor R_c from Equation (1) and mentioned in Ref. [54] the plastic moment of the tube wall m_p that is given, according to [7], as:

$$m_p = \frac{t^2 \sigma_y}{4} \tag{18}$$

whereas for the ship, a value κ_s is assumed from the deformation behaviour as defined in Section 3. For κ_s only the deformed bow parts are considered. Thus, for brace impact in cases 19 and 20 $\kappa_s = \kappa_b$ (Fig. 11) of the respective ship model. The differentiation between the cases is made for the influence of the buckling of braces near the impact point and for the collision type (joint or span impact).

Each pair of points corresponding to a different case is plotted symmetrically according to the respective parameter. While the energy dissipation is characterised in terms of the local response of the platform for κ_s/m_p and R_c, for the ratio κ_s/κ_i the structure global behaviour assumes higher preponderance. Although in each pair of graphics some trends can be speculated, the dispersion that can be observed relative to these trends increases the degree of uncertainty if any of the tried assumptions were to be considered. The use of R_c confirms the results from Ref. [54] that (for model 'S2') a value of $R_c > 1.6$–1.7 MN should be sufficient to cause the bulb to crush without significant denting of the tube. If the ship is assumed to be stronger, such as model 'S10', then a slight increase of R_c would become more appropriate, even considering the stress distribution from the respective contact areas. The dissipation can however occur in other ways when the compactness requirement is fulfilled. In case 15, for instance, the installation is able to dissipate ~45% of the total energy, owing to the platform dimensions and overall elastic response of the frame. Nevertheless, it must be noted that such case corresponds to an impact scenario where the joint is directly hit by the bulb. In turn, the buckling of adjacent braces does not seem to affect the trend for when R_c is used.

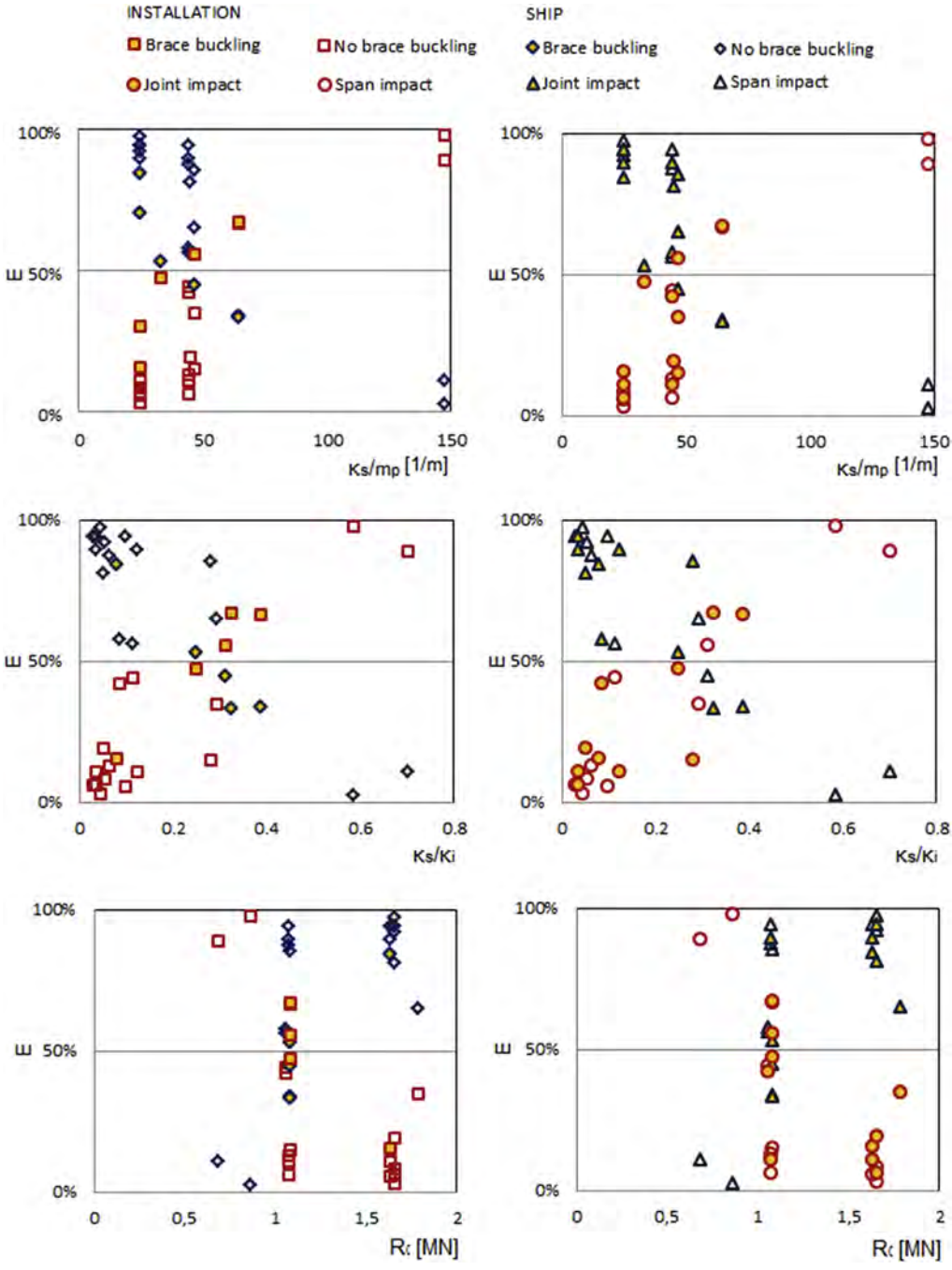

Fig. 18. Energy dissipation based on structural relative strength.

By considering the ratio κ_s/m_p some attention is drawn to the variation of the ship stiffness. The influence of the tube thickness is also emphasized, rather than its diameter or even length. In fact, if Equations (1)–(5) are taken into account, it is clear that more energy is dissipated by a tube when its thickness increases rather than with the decrease of the D/t ratio through the decrease of the diameter. The respective graphics show some similarity with the qualitative curves of energy dissipation vs. the relative strength [3], being that for $30 < \kappa_s/m_p < 60$ the platform can dissipate from ~0 to ~50% of the energy. Again, this arises from the joint impacts where the frame global deformation plays an important role. Some lack of data is found for $65 < \kappa_s/m_p < 145$, mainly due to the tested thickness values on the platforms that range from 45 mm to 70 mm for the legs and 15 mm–20 mm for braces. If for the ship case the length H of the folds that also contribute for the energy absorption (Equations (7) and (8)) is influenced by size and stiffening of the plates, for the installation case, the plate thickness t almost determines whether the tube wall gets dented as well as it contributes more than any other geometrical factor to the platform local stiffness. This affirmation is of course valid for the ratios L/D and D/t and their range of values for the cases being analysed ($8 < L/D < 28$ and $17 < D/t < 40$), even though these values can often be adopted in the design of the steel frames of offshore facilities. For κ_s/κ_i, where more emphasis is given to the platform elastic stiffness at the collision point, the plot assumes approximately a linear trend, although with some dispersion due to either local denting or brace

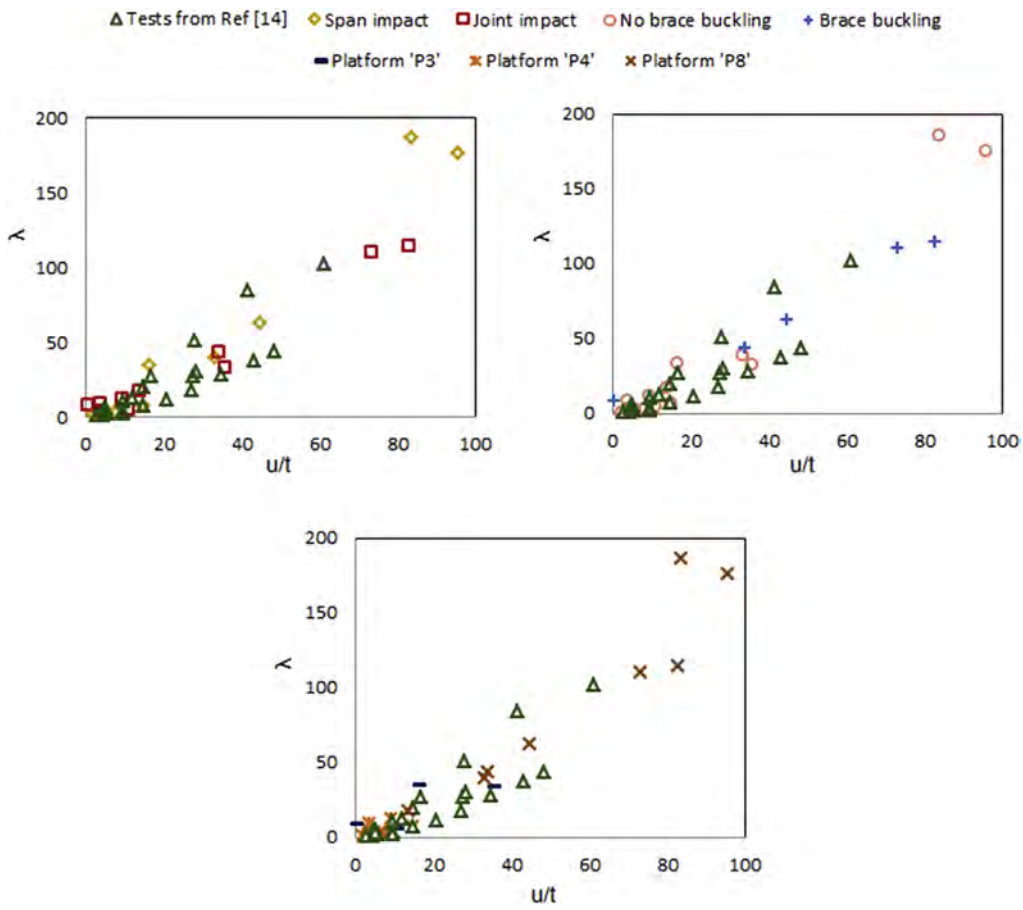

Fig. 19. Dimensionless horizontal displacement struck zone versus dimensionless strain energy of installation.

buckling in the smaller platform models. Therefore, κ_s/κ_i is affected by the platform dimensions, directly related to the frame energy.

It must also be noted that the results plotted in Fig. 18 only indicate the relative strain energy. The absolute values of internal energy necessary to collapse a member of an offshore platform or provoke certain damage on a ship hull shall be provided by an independent assessment of the respective collision scenario that is beyond the scope of this study.

The above observations lead to the conclusion that the adoption of a coupled analysis is very limited, i.e., other factors such as the platform size or the impact location should be taken into account prior to defining the right parameter or stiffness ratio for the estimation of the energy dissipation. Accounting for the influence of brace buckling, impact location or global frame deformation, the dimensionless energy of the platform are also analysed based on Equation (6). The numerical cases are presented and compared in Fig. 19 by means of the relationship between the dimensionless energy λ (Equation (6)) of the platform and the dimensionless displacement u/t of the platform struck zone. For comparison, the testing data from Ref. [14] for isolated tubular members within a range of different dimensions, boundary conditions and axial loading are also included in the Figure. The numerical simulation cases performed in the current study are grouped according to the platform type, impact type (span or joint) and the contribution (or not) of any adjacent braces (leg impact) with plastic deformation to the platform energy dissipation.

For the calculation of λ in scenarios of collision with a joint, the total length L is taken as the adjacent leg span. This assumption is made since for the joint impact cases the ship bulb not only hits the joint, its upper part is also usually in contact with the span. Parameter P_u, as referred in Equation (6), stands for the plastic limit load applied at the mid-length of a clamped tube. Such value varies according to, for instance, the tube boundary conditions, where for pinned ends it is reduced to half. The length considered for the estimation of the dimensionless energy (Equation (6)) of the platform is described as L_1, according to Fig. 20. For the full platform models, the application of Equation (6) that establishes the relationship between the displacement of the contact area considers, besides the strain energy of the struck tube, any additional energy amounts dissipated over the remaining structure through the different mechanisms (brace buckling, frame vibrations, etc.). This includes the following particularities: firstly, the tube length associated with flexural behaviour might extend to the lower adjacent span of the leg (L_2 in Fig. 20). Despite not so significant, the contribution of the strain energy due to bending might not be restricted to only one leg span; the second point is the fact that brace buckling due to axial forces also contributes to the total energy absorbed by the platform and included in Equation (6), which mainly takes into account the effects due to local denting and beam bending; the

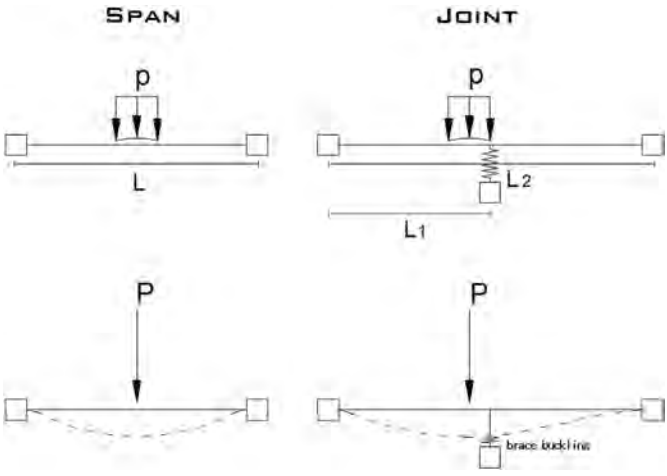

Fig. 20. Substructures considered for definition of P_u.

same is observed for the frame overall displacement, that contributes to the total displacement measured at the contact point and with energy amounts that can become very significant depending on the platform type, as seen above. The contribution of the bent brace due to local axial forces is not significantly reflected in the linear relationship between λ and u/t, contrary to the platform size that can be closely associated to the frame elastic energy. This reinforces the idea that performing a single analysis that accounts for both local and global mechanisms, aiming to estimate the energy dissipation of the complete system (ship + platform), does not appear possible. On the other hand, the evaluation of the platform response seems to be possible with acceptable accuracy if preliminary assessment of the platform local strength at the impact point for the respective impact action is carried out. The uncoupled analyses of SDOF for global frame response and/or hand calculations for the tube flexural deformation are then performed according to the predicted/pre-established conditions.

6. Conclusion

In this study the results of a series of detailed FEM simulations of the impact between vessels and fixed offshore steel platforms are discussed with respect to the energy dissipation. Predicting the size increase of supply vessels in the near future, as well as possible ship impacts involving higher energy amounts than those usually considered by the current design practice, both loading curves and simplified equivalent systems representative for ships up to 25,000 DWT were derived from the FEA. Aspects such as the steel grades or the scantling size variation were considered in the analyses for the purpose of broadening the scope of ship types/categories.

Because the platform response to strong impacts might involve yielding of other members besides those directly affected by the contact with the ship, different scenarios were defined involving different plastic mechanisms and possible combinations among these mechanisms. It has been revealed that the plastic energy absorbed by the platform can be evaluated and will mostly depend on the impact area, but also include contributions from deformations that can take place in adjacent members. The thickness of the installation tubes, in particular of the struck tubes, has been shown to have some degree of connection to the platform internal energy after-impact and therefore the plastic moment of the tube walls can be used to describe the platform relative strength, depending on the platform dimensions as well, since elastic strain energy gains importance for big steel platforms and for joint impacts. The interaction between the vessel and the platform appears to be important, particularly in cases in which the energy share is closer to 50/50 corresponding to significant energy amounts and significant plastic deformation/damage in both structures. For the ship range considered, these are observed mainly when the tube thickness is in 45 mm $< t <$ 70 mm.

In conclusion, if plastic analysis is to be considered in the design practise against extreme accidental loads from higher energy ship impacts, the present results might provide some good indications especially regarding the global integrity of the structure and the ship-installation interaction. However, this can be better complemented with additional investigation on the individual failure of members based on energy absorption since that is only addressed generally in the current study.

Acknowledgement

The authors would like to thank The University of Western Australia (UWA) and Australian Research Council (PG10100033) for providing scholarship and research funds to the first author to pursue his PhD study in UWA and carry out this research.

Appendix

Structural details of vessels and offshore installations analysed.
Ship '*S20*'

General dimensions
Length – 174 m

Breadth – 29.5 m
Height – 17 m
Mass (+5% of surge added mass included) – 28,200 ton
Scantlings of unstiffened bow (with smeared out thickness of equivalent stiffened bow with large scantlings)
1st, 3rd and 4th decks – plate thickness 15 mm
2nd and 5th decks – plate thickness 19 mm
Lower and upper side shell – plate thickness 42 mm
Mid side shell – plate thickness 21 mm
Girders – 11 mm
Frames – spacing 0.7 m, 12 mm
CL girder (bottom) – 16 mm

Ship 'S10'

General dimensions
Length – 130 m
Breadth – 19 m
Height – 15 m
Mass (+5% of surge added mass included) – 13,300 ton
Radius of inertia for yaw – 37.0 m
Normal scantlings
Longitudinals – spacing 0.8m, L500 × 100 × 9/11 mm
1st, 2nd and 4th decks – plate thickness 11 mm
3rd and 5th decks – plate thickness 13 mm
Lower and upper side shell – plate thickness 13 mm
Mid side shell – plate thickness 11 mm
CL girder – L1400 × 250 × 11 × 13 mm
Larger scantlings
Longitudinals – spacing 0.8 m, L500 × 100 × 11/11 mm
1st, 2nd and 4th decks – plate thickness 11 mm
3rd and 5th decks – plate thickness 13 mm
Lower and upper side shell – plate thickness 18 mm
Mid side shell – plate thickness 13 mm
CL girder – L1400 × 250 × 14 × 18 mm
Scantlings of unstiffened bow (with smeared out thickness of equivalent stiffened bow with larger scantlings)
1st, 2nd and 4th decks – plate thickness 16 mm
3rd and 5th decks – plate thickness 18 mm
Lower and upper side shell – plate thickness 26 mm
Mid side shell – plate thickness 21 mm
Girders – L1400 × 250 × 14 × 18 mm

Ship 'S2'

General dimensions
Length – 63.5 m
Breadth – 13.3 m
Height – 6.3 m
Mass (+5% of surge added mass included) – 3000 ton
Normal scantlings
Longitudinals – spacing 0.8 m
Plate thickness – 9 mm

Shell thickness – 11 mm
Larger scantlings
Longitudinals – spacing 0.8 m
Plate thickness – 9 mm
Shell thickness – 14 mm

Platform 'P3'
Platform 'P4'
Platform 'P8'
*The thickness of the tubular members for all the platforms is variable according to the collision cases.

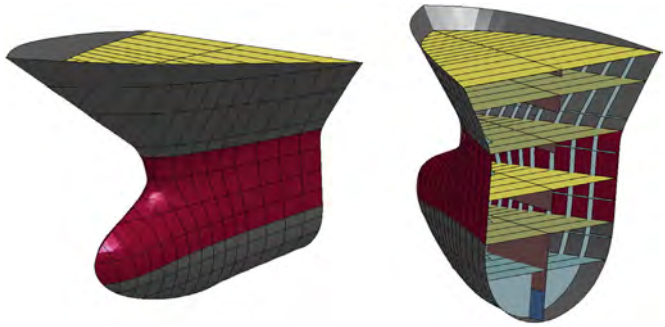

Fig. A1. Bow 'S20'.

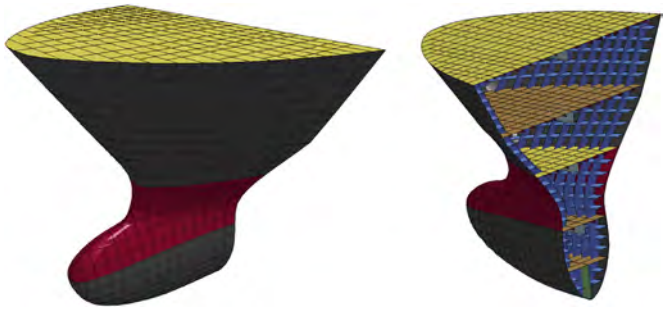

Fig. A2. Bow 'S10'.

Fig. A3. Bow 'S2'.

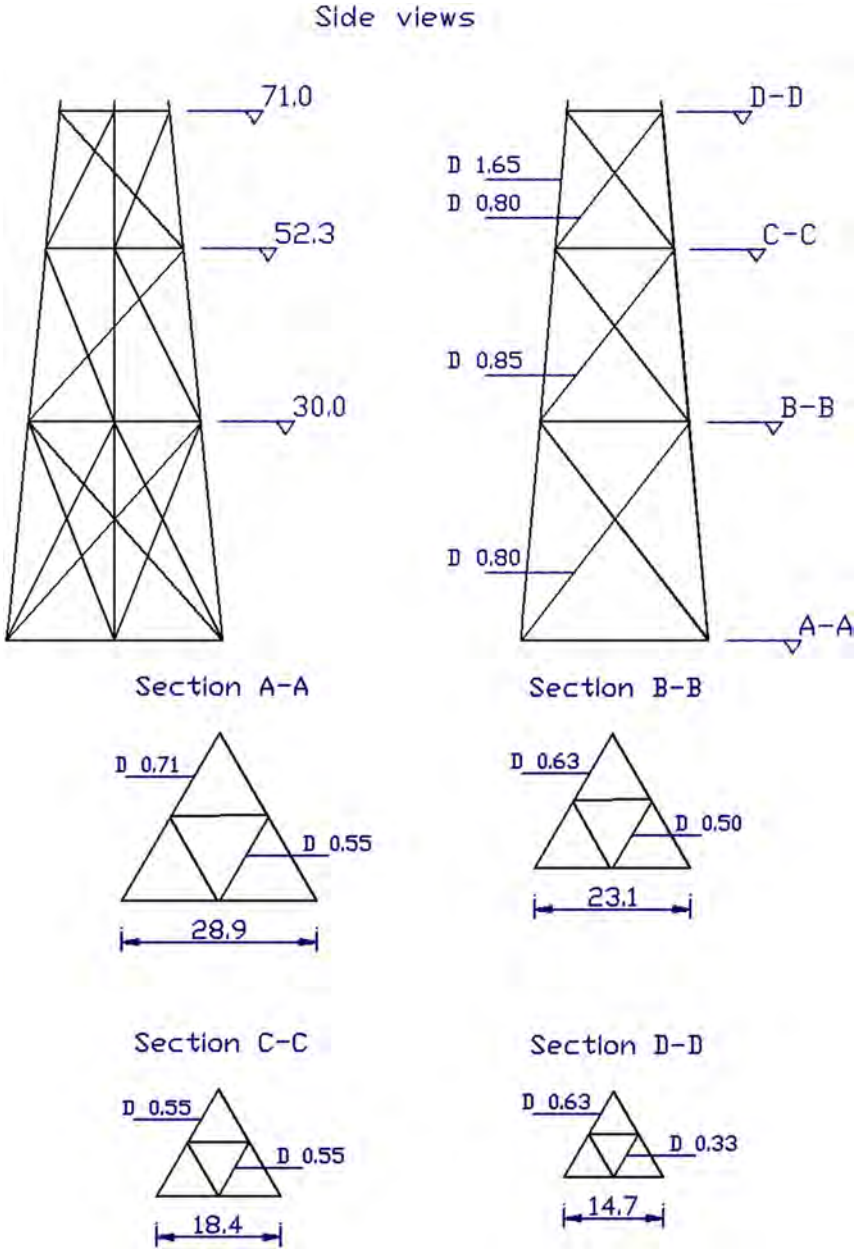

Fig. A4. Platform 'P3' (Dimensions in meters).

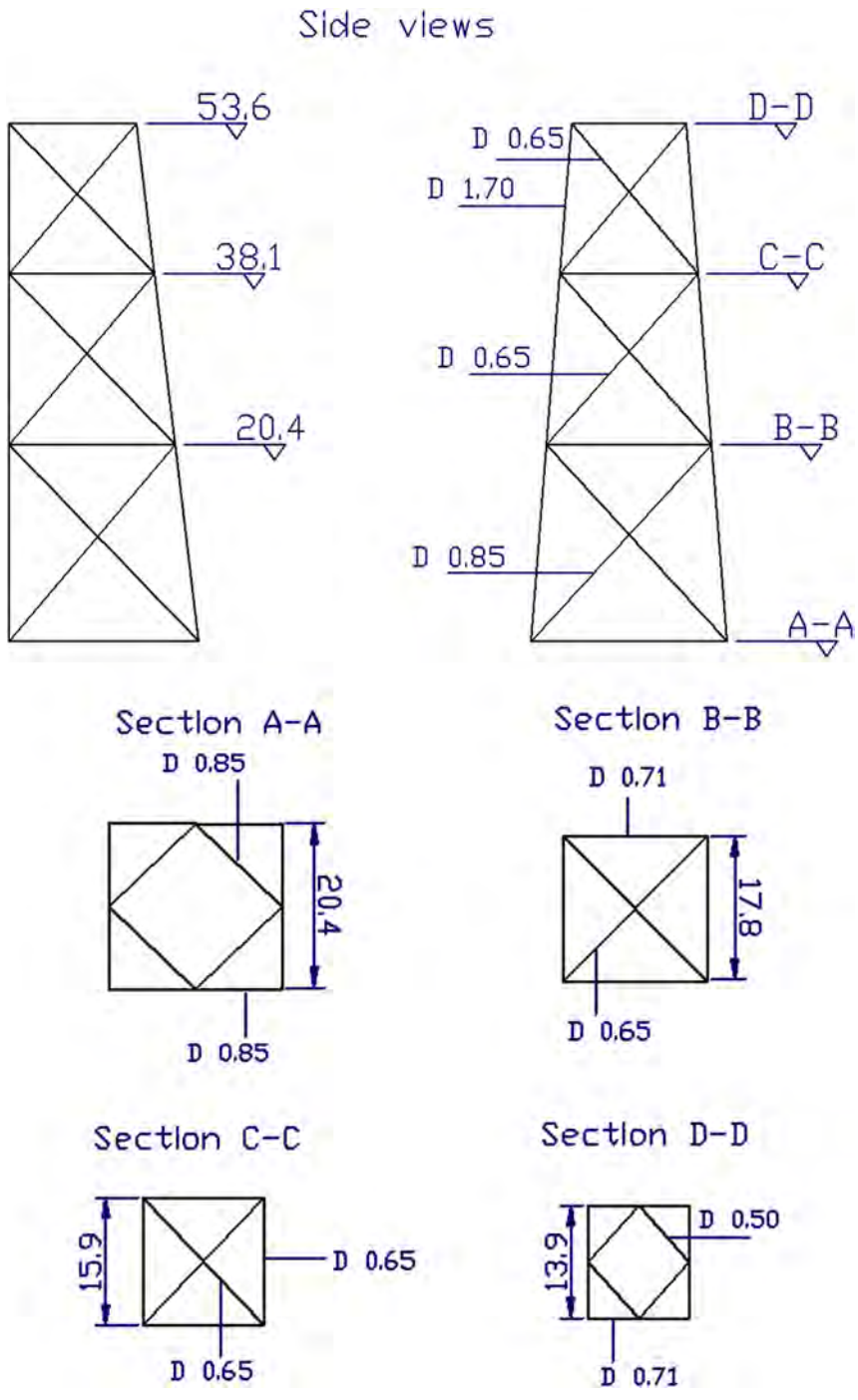

Fig. A5. Platform 'P4' (Dimensions in meters).

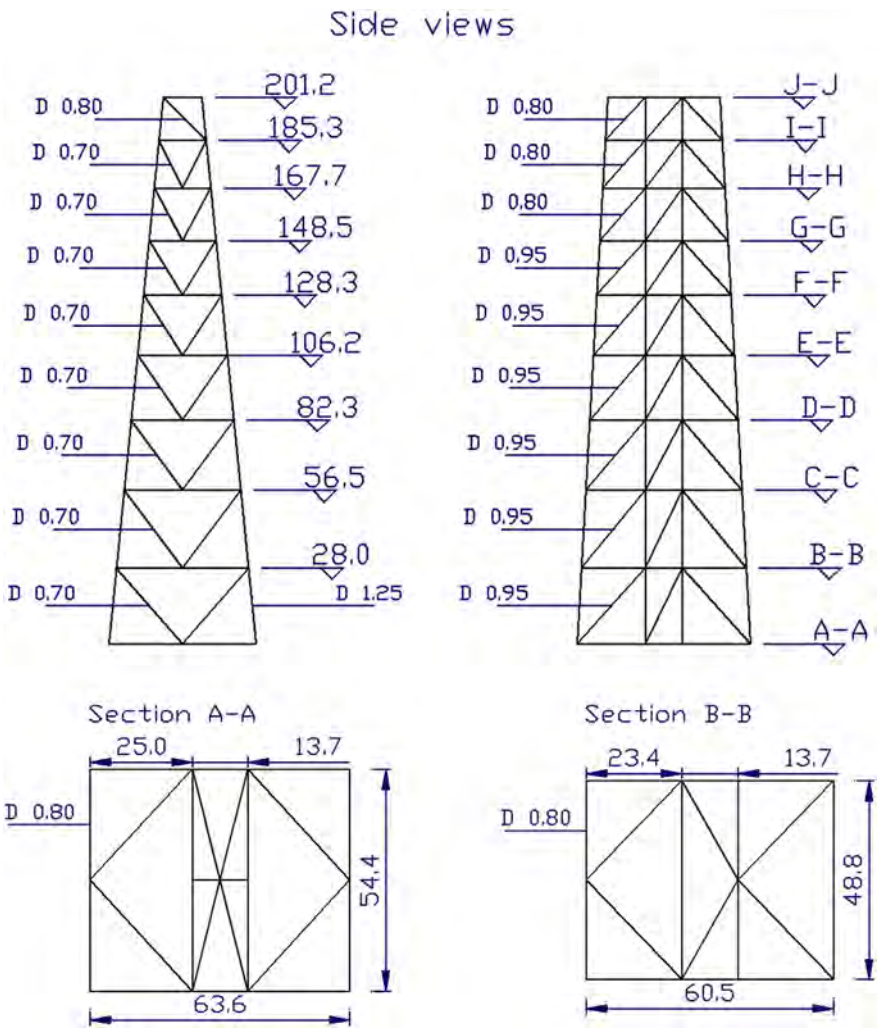
Side views
201.2
185.3
167.7
148.5
128.3
106.2
82.3
56.5
28.0
D 0.80
D 0.70
D 0.70
D 0.70
D 0.70
D 0.70
D 0.70
D 0.70
D 0.70
D 1.25
J-J
I-I
H-H
G-G
F-F
E-E
D-D
C-C
B-B
A-A
D 0.80
D 0.80
D 0.80
D 0.95
D 0.95
D 0.95
D 0.95
D 0.95
D 0.95
Section A-A
25.0
13.7
D 0.80
54.4
63.6
Section B-B
23.4
13.7
D 0.80
48.8
60.5

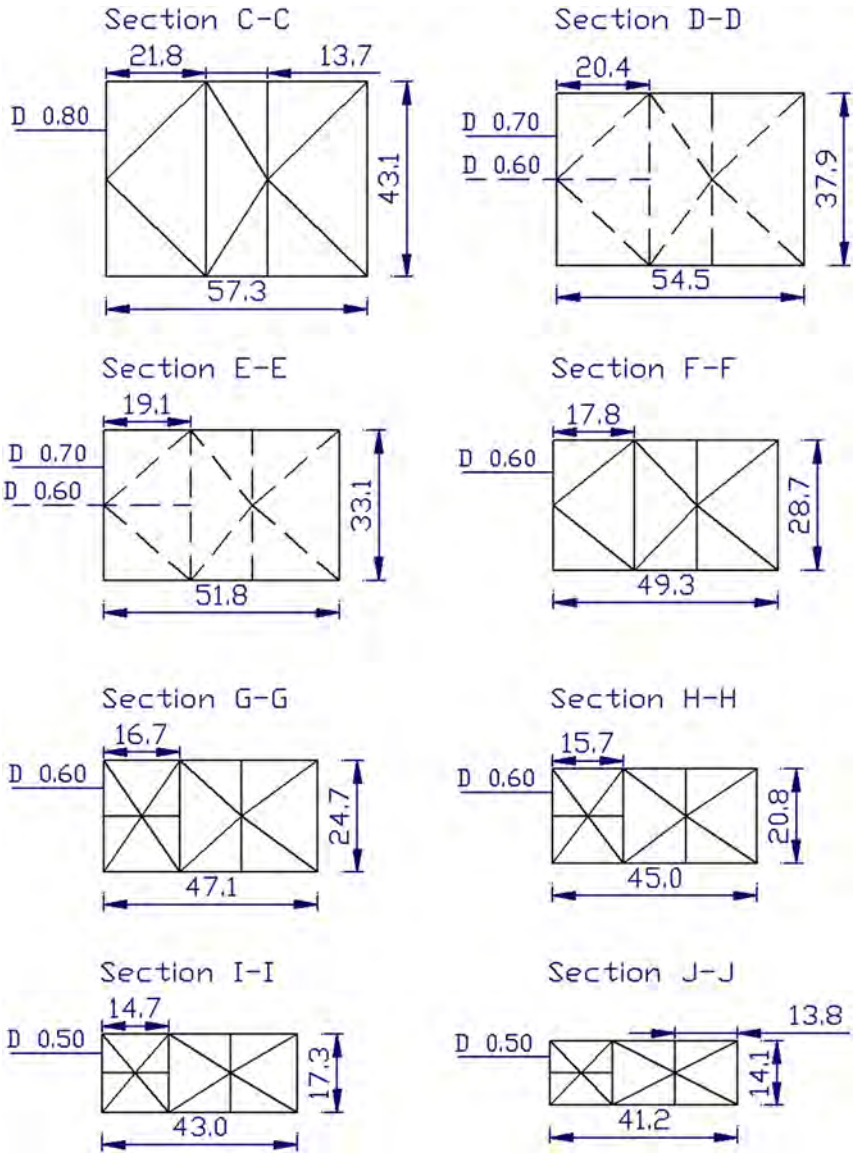

Fig. A6. a. Platform 'P8' (Dimensions in meters). b. Platform 'P8' (Dimensions in meters).

References

[1] Sii HS, Wang J, Ruxton T. A statistical review of the risk associated with offshore support vessel/platform encounters in UK waters,. J Risk Res 2003;6(2):163–77.
[2] Mather A. Offshore engineering – an introduction. London: Witherby & Company Limited; 1995.
[3] Veritas Det Norske. Design against accidental loads. Recommended practise DNV-RP-C204. 2010.
[4] ISO 19902:2007. Petroleum and natural gas industries – fixed steel offshore structures. 1st ed. International Organization Standardization; 2007.
[5] American Petroleum Institute. Recommended practice for planning, designing and constructing fixed offshore platforms – working stress design, RP 2A WSD. 21st ed. 2000. Washington, DC., USA.
[6] Robson JK. Ship/platform collision incident database (2001). Culham: HSE Books; 2003. Research Report RR053.

[7] Furnes O, Amdahl J. Ship collisions with offshore platforms. Hamburg: Intermaritec' 80; 1980. p. 310–28.
[8] Ellinas CP, Walker AC. Damage on offshore tubular bracing members. In: Proc. IABSE colloquium on ship collision with bridges and offshore structures, vol. 42; 1985. p. 253–61. Copenhagen.
[9] Ruggieri C, Ferrari JA. Structural behaviour of dented tubular members under lateral loads. J Offshore Mech Arctic Eng 2004;126:191–7.
[10] Zeinoddini M, Harding J, Parke GAR. Axially pre-loaded steel tubes under lateral loads. Int J Mech Sci 2006;48:1080–94.
[11] Jones N, Birch RS. Influence of internal pressure on the impact behaviour of steel pipelines. J Press Vessel Tech 1996;118:464–71.
[12] Jones N, Birch RS. Low-velocity impact of pressurised pipelines. Int J Impact Eng 2010;37:207–19.
[13] Oliveira JG. The behaviour of steel offshore structures under accidental collisions. In: Offshore Technology Conf., OTC 4136; 1981. p. 187–98. Houston, USA.
[14] Travanca J, Hao H. Numerical analysis of steel tubular member response to ship Bow impacts. Int J Impact Eng 2014;64:101–21.
[15] Wierzbicki T, Abramowicz W. On the crushing mechanics of thin-walled structures. J Appl Mech 1983;50:727–34.
[16] Abramowicz W, Jones N. Dynamic axial crushing of circular tubes. Int J Impact Eng 1984;2(3):263–81.
[17] Wierzbicki T, Bhat SU, Abramowicz W, Brodkin D. Alexander revisited – a two folding elements model of progressive crushing of tubes. Int J Solids Struct 1992;29(4):3269–88.
[18] Alexander JM. An approximate analysis of the collapse of thin cylindrical shells under axial loading. Q. J Mech Appl Math 1960;13:10–5.
[19] Johnson W. Impact strength of materials. London, Crane Russak, New York: Edward Arnold; 1972.
[20] Karagiozova D, Alves M. Transition from progressive buckling to global bending of circular shells under axial impact – Part I: experimental and numerical observations. Int J Solids Struct 2004;41:1565–80.
[21] Karagiozova D, Alves M. Transition from progressive buckling to global bending of circular shells under axial impact – Part II: experimental and numerical observations. Int J Solids Struct 2004;41:1581–604.
[22] Karagiozova D, Jones N. Dynamic elastic-plastic buckling phenomena in a rod due to axial impact. Int J Impact Eng 1996;18:919–47.
[23] Karagiozova D, Jones N. On the mechanics of the global bending collapse of circular tubes under dynamic axial load – dynamic buckling transition. Int J Impact Eng 2008;25:397–424.
[24] Karagiozova D, Alves M. Dynamic elastic-plastic buckling of structural elements: a review. Appl Mech Rev 2008;61:1–25.
[25] unctad.org/en/publicationslibrary/rmt2013_en.pdf. Review of maritime transport. UNCTAD/RMT/2013. United Nations Publication; 2013.
[26] The Overseas Coastal Area Development Institute of Japan. Technical standards and commentaries for port and harbour facilities in Japan. Japan: Daikousha Printing Co., Ltd; 2009.
[27] Visser W. Ship collision and capacity of brace members of fixed steel offshore platforms. Research Report RR220. Houten: HSE Books; 2004.
[28] Lehmann E, Peschmann J. Energy absorption by the steel structure of ships in the event of collisions. Mar Struct 2002;15(4–5):429–41.
[29] Liu Z, Amdahl J, Løset S. Integrated analysis of Ship/Iceberg collision. In: Proceedings of the International Conference on Collision and Grounding of Ships; 2010. p. 173–8. Espoo, Finland.
[30] Kitamura O. FEM Approach to the simulation of collision and grounding damage. Mar Struct 2002;15(4–5):403–28.
[31] Yagi S, Kumamoto H, Muragishi O, Takaoka Y, Shimoda TA. Study on collision buffer characteristic of sharp entrance angle bow structure. Mar Struct 2009;22:12–23.
[32] Yang PDC, Caldwell JB. Collision energy absorption of ships' bow structures. Int J Impact Eng 1988;7(2):181–96.
[33] Paik JK, Chung JY, Paik YM. On dynamic/impact tensile strength characteristics of thin high tensile steel materials for automobiles. Korean Soc Automot Eng 1999;7:268–78.
[34] Cowper JR, Symonds PS. Strain-hardening and strain-rate effects in the impact loading of cantilever beams. Technical report no. 28. Providence, Ri, USA: Division of Applied Mathematics, Brown University; 1957.
[35] Paik JK. Practical techniques for finite element modelling to simulate structural crashworthiness in ship collisions and grounding (Part I: theory). Ships Offshore Struct 2007;2(1):69–80.
[36] Paik JK. Practical techniques for finite element modelling to simulate structural crashworthiness in ship collisions and grounding (Part II: verification). Ships Offshore Struct 2007;2(1):81–5.
[37] Minorsky VU. An analysis of ship collisions with reference to nuclear power plants. J Ship Res 1959;3(2):1–4.
[38] Gerard G. The crippling strength of compression elements. J Aeronaut Sci 1958;25(1):37–52.
[39] Amdahl J. Energy absorption in ship-platform impacts. Dr. Ing. Thesis, Report No. UR-83–84. Trondheim: The Norwegian Institute of Technology; 1983.
[40] Roccotelli S. Concerning experimental research applied to naval construction. Naval ng. Jnl 1965;77:705–14.
[41] Euratom. Collision tests with ship models. Euratom Report Eur 4560 E. Luxemburg. 1971.
[42] Kagami, et al. Research on collision resisting construction of the sides of ship. Report No. 2, Mitsubishi Nippon Industries, Technical Review 2. 1961.
[43] Wierzbicki T [chapter 3]. In: Jones N, Wierzbicki T, editors. Crushing behaviour of plate intersections, structural crashworthiness. London: Butterworth and Co; 1983.
[44] Paik JK, Chung JY, Chun MS. On quasi-static crushing of a stiffened square tube. J Ship Res 1996;40:258–67.
[45] Paik JK, Pedersen PT. Ultimate and crushing strength of plated structures. J Ship Res 1995;39(3):250–61.
[46] Yamada Y, Pedersen P. A benchmark study of procedures for analysis of axial crushing of bulbous bows. Mar Struct 2008;21:257–93.
[47] Saul R, Svensson H. Means of reducing consequences of ship collisions with bridges and offshore structures. I ABSE colloquium on ship collision with bridges and offshore structures. 1983. Copenhagen.
[48] US Department of Transportation. In: Federal highway administration, guide specification and commentary for vessel collision design of highway bridges, vol. I; 1990. Publication No. FHWA-RD-91–006.

[49] Pedersen PT, Valsgard S, Olsen D, Spangenberg S. Ship impacts: bow collisions. Int J Impact Eng 1993;13(2):163–87.
[50] Valsgard S, Pettersen E. Simplified non-linear analysis of ship/ship collisions. Nor Marit Res 1982;3:2–17.
[51] Bach-Gansmo O, Valsgard S. Simplified stiffness evaluation of a bulbous ship bow. 1981. Progress report No. 1, DNV, Report No. 81–0437 (Rev. no. 1 of 17.02.82).
[52] Billingham J, Sharp JV, Spurrier J, Kilgallon PJ. Review of the performance of high strength steels used offshore, research report RR105. Cranfield: HSE Books; 2003.
[53] Travanca J, Hao H. Dynamics of steel offshore platforms under ship impact. Appl Ocean Res 2014;47:352–72.
[54] Storheim M, Amdahl J. Design of offshore structures against accidental ship collisions. Mar Struct 2014;37:135–72.